Climate Dynamics
https://doi.org/10.1007/s00382-021-05667-2

Temperature and precipitation projections for the Antarctic Peninsula over the next two decades: contrasting global and regional climate model simulations

Deniz Bozkurt[1,2,3,4] · **David H. Bromwich**[5] · **Jorge Carrasco**[6] · **Roberto Rondanelli**[2,7]

Received: 16 June 2020 / Accepted: 20 January 2021

Abstract
This study presents near future (2020–2044) temperature and precipitation changes over the Antarctic Peninsula under the high-emission scenario (RCP8.5). We make use of historical and projected simulations from 19 global climate models (GCMs) participating in Coupled Model Intercomparison Project phase 5 (CMIP5). We compare and contrast GCMs projections with two groups of regional climate model simulations (RCMs): (1) high resolution (15-km) simulations performed with Polar-WRF model forced with bias-corrected NCAR-CESM1 (NC-CORR) over the Antarctic Peninsula, (2) medium resolution (50-km) simulations of KNMI-RACMO21P forced with EC-EARTH (EC) obtained from the CORDEX-Antarctica. A further comparison of historical simulations (1981–2005) with respect to ERA5 reanalysis is also included for circulation patterns and near-surface temperature climatology. In general, both RCM boundary conditions represent well the main circulation patterns of the historical period. Nonetheless, there are important differences in projections such as a notable deepening and weakening of the Amundsen Sea Low in EC and NC-CORR, respectively. Mean annual near-surface temperatures are projected to increase by about 0.5–1.5 °C across the entire peninsula. Temperature increase is more substantial in autumn and winter (∼ 2 °C). Following opposite circulation pattern changes, both EC and NC-CORR exhibit different warming rates, indicating a possible continuation of natural decadal variability. Although generally showing similar temperature changes, RCM projections show less warming and a smaller increase in melt days in the Larsen Ice Shelf compared to their respective driving fields. Regarding precipitation, there is a broad agreement among the simulations, indicating an increase in mean annual precipitation (∼ 5 to 10%). However, RCMs show some notable differences over the Larsen Ice Shelf where total precipitation decreases (for RACMO) and shows a small increase in rain frequency. We conclude that it seems still difficult to get consistent projections from GCMs for the Antarctic Peninsula as depicted in both RCM boundary conditions. In addition, dominant and common changes from the boundary conditions are largely evident in the RCM simulations. We argue that added value of RCM projections is driven by processes shaped by finer local details and different physics schemes that are introduced by RCMs, particularly over the Larsen Ice Shelf.

Keywords Model evaluation · Antarctica · Dynamical downscaling · Climate change · Added value · Temperature extremes · Larsen Ice Shelf

✉ Deniz Bozkurt
deniz.bozkurt@uv.cl

[1] Department of Meteorology, University of Valparaíso, Valparaíso, Chile

[2] Center for Climate and Resilience Research (CR)2, Santiago, Chile

[3] Centro de Estudios Atmosféricos y Astroestadística, Universidad de Valparaíso, Valparaíso, Chile

[4] Centro de Investigación y Gestión de Recursos Naturales, Universidad de Valparaíso, Valparaíso, Chile

[5] Polar Meteorology Group, Byrd Polar and Climate Research Center, The Ohio State University, Columbus, OH, USA

[6] Centro de Investigación GAIA Antártica, Universidad de Magallanes, Punta Arenas, Chile

[7] Department of Geophysics, University of Chile, Santiago, Chile

Published online: 08 February 2021

1 Introduction

West Antarctica, especially the Antarctic Peninsula (~ 63 to 70 °S, Fig. 1a), has been one of the fastest warming regions on Earth since the 1950s (Marshall et al. 2006; Ding et al. 2011; Bromwich et al. 2013, 2014; Cape et al. 2015; Turner et al. 2016). This long-term warming trend has caused abrupt changes in the Peninsula's ecosystem and cryosphere (e.g., Scambos et al. 2004; Rignot et al. 2004; Convey and Smith 2006). On the other hand, due to the natural variability of climate, some parts of Antarctica including the Antarctic Peninsula, have experienced a cooling trend since the late 1990s (Carrasco 2013; Turner et al. 2016, 2020b; Oliva et al. 2017; Jones et al. 2019). Nonetheless, even during this recent cooling period, some parts of the Antarctic Peninsula exhibited persistent warming trends particularly in autumn season that can have an important effect on the fate of ice sheet surfaces in the warming areas (Bozkurt et al. 2020). In addition, Turner et al. (2020a) showed that in 2016/17 the extent of summer sea ice in the Weddell Sea dropped to a near-record level in the satellite era, which starts in late 1978. Therefore, the question of how the climate conditions of the Antarctic Peninsula will change in the near future needs to distinguish between long-term anthropogenic climate change signal and short term fluctuations due to natural variability.

In spite of the importance of such distinction between long- and recent-term climate variability, efforts to conduct future climate projections on the Antarctic Peninsula remain largely incomplete. Most of the climate change studies are based on continental scale projections obtained from the global climate models (GCMs) with coarse spatial resolutions (~ 100 to 200 km). Based on these projections, there is a consensus among the GCMs from the Coupled Model Intercomparison Project phase 5 (CMIP5) (Taylor et al. 2012) that suggests a very likely increase in near-surface temperature on the Antarctic continent under the RCP8.5 scenario. A further increase of 0.5 °C beyond the present-day average global surface temperature will lead to dramatic impacts on a variety of organisms in western Antarctic Peninsula (Hoegh-Guldberg et al. 2018). On the other hand, Jones et al. (2019) showed that the CMIP5 models warm Antarctica too rapidly (factor of 1.5–2 times, depending on analysis approach) indicating substantial uncertainty in these projections although multidecadal variability adds uncertainty. Projected warming is likely to lead to an increase in precipitation in Antarctica (Bracegirdle et al. 2008; Frieler et al. 2015; Palerme et al. 2017). However, models differ widely in their projections of temperature and precipitation. For that reason, there are inconsistencies and uncertainties between the models that prevent a correct reproduction of some regional impacts such as surface mass balance of West Antarctica (e.g., Naughten et al. 2018). The degree of these inconsistencies and uncertainties can get worse when going from regional to local scales such as Larsen Ice Shelf in the Antarctic Peninsula.

On one hand, GCMs are the main tool for climate change and future projections of the Antarctic continent by having the capability to resolve different components of the climate system as well as important large-scale circulation patterns such as El Niño–Southern Oscillation (ENSO) and Southern Annular Mode (SAM). On the other hand, GCMs generally

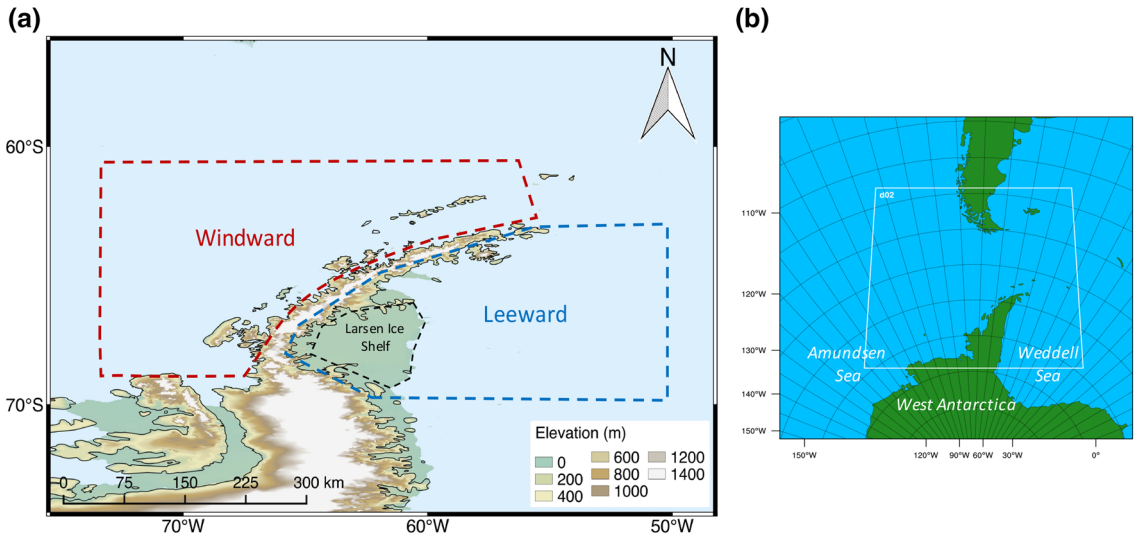

Fig. 1 **a** Study region of the Antarctic Peninsula. The red and blue dashed lines correspond to the windward and leeward sides of the peninsula, respectively. The black dashed border identifies the Larsen Ice Shelf for melt days and rain days analysis. **b** Domain setup at 15 km resolution (d02, white border) used for PWRF simulations

tend to have large uncertainties in reproducing atmospheric teleconnection patterns such as the South Pacific teleconnection (e.g., Wilson et al. 2016). In addition to large-scale uncertainties, GCMs largely fail to represent regional to local-scale features due to their coarse spatial resolutions. For instance, the north-south mountain range in the Antarctic Peninsula acts as an orographic obstacle to the westerlies, which leads to a relatively mild and humid marine climate on the west coast and a cooler continental climate on the east coast (King and Turner 2009). In a similar manner, due to the orographic effect, the west coast of the Peninsula receives greater precipitation compared to the rest of the Peninsula. In addition, due to the presence of the orographic barrier, the eastern coasts of the Peninsula can be affected by dry and warm descending winds (Elvidge et al. 2015). Given these important local-scale features, the GCMs can miss considerable climate gradients imposed by the topography over the Peninsula. In this respect, dynamical downscaling efforts via regional climate models (RCMs) using the GCMs (or other source such as reanalysis) as lateral boundary conditions can provide added value since RCMs incorporate physical processes that are typical of the regional scale, allowing the diagnosis of climatic phenomena and their change in complex and extreme regions such as the Antarctic Peninsula.

For instance, Bozkurt et al. (2020) demonstrated the added value introduced by the high resolution (15 km) RCM in capturing the recent temperature trends over the Antarctic Peninsula. In addition, by using a 14 km resolution RCM simulation Van Lipzig et al. (2008) showed the formation of precipitation shadow on the eastern side of the Antarctic Peninsula due to the significant orographic barrier (dryness due to adiabatically descending air in the lee side), which is not captured at 55 km resolution (Van Den Broeke and Van Lipzig 2004). Nonetheless, despite the improvements and added value, the RCMs tend to inherit systematic errors through the boundary conditions. Furthermore, the complexity of climate features shaped by both large- and local-scale factors can increase the uncertainties in the GCM-RCM model chain. This is particularly important for the Antarctic Peninsula, because the large-scale climate component of the Antarctic Peninsula is largely controlled by westerlies (e.g., SAM) as well as mid-latitude baroclinic systems and even remote tropical sea surface temperature (SST) forcing (Marshall et al. 2006; Bromwich et al. 2013; Hosking et al. 2013; Clem et al. 2019). Therefore, a comprehensive evaluation and comparison of the GCM-RCM chain is important to assess the robustness of climate change projections over the Antarctic Peninsula.

Given that little attention has been paid to assess regional climate change projections of the Antarctic Peninsula and to compare GCM and RCM based climate change projections, our main objective is twofold: first, to provide near future (2020–2044) temperature and precipitation projections of the Antarctic Peninsula under RCP8.5 scenario obtained from 19 GCMs participating CMIP5 and 2 RCMs at high (15 km) and medium resolution (50 km); second to compare GCMs and RCMs as well as RCMs and their driving fields in order to assess the robustness of the projections. This study also evaluates the historical simulations with respect to ERA5 for the period 1981–2005 in terms of circulation patterns and near-surface temperature. Section 2 provides a description of the data and methodology used in this study. Section 3 presents the results in three aspects: (1) a brief evaluation of the historical simulations, (2) projected changes in circulation patterns, temperature and precipitation, and (3) projected changes in extreme days (i.e., melt days and rain days). Sections 4 and 5 discusses and summarizes the results, respectively.

2 Data and methodology

2.1 Reanalysis

In this work, we used the European Centre for Medium-Range Weather Forecasts (ECMWF) ERA5 reanalysis that combines large amounts of historical observations into global estimates using advanced modeling systems and data assimilation, i.e., Integrated Forecasting System (IFS) CY41R2 (C3S 2017; Hersbach et al. 2020). ERA5 has a spatial resolution of 0.25 ×0.25° (~ 30 km) and vertical resolution of 137 levels from the surface to a height of 80 km. The reanalysis data extend from 1979 to the present, and in order to have the consistency with the historical simulations, we used the period 1981–2005 for the analysis. We used near-surface air temperature data to contrast the simulations for the historical period. In addition, we included mean sea level pressure (MSLP) and 850 hPa zonal winds in the analysis in order to compare circulation patterns with the simulations.

Although reanalysis data yield complete and continually updated global gridded climatic data, they can still suffer from important biases over the remote regions such as Antarctica. Nonetheless, previous studies reported some improvements in the performance of ERA5 over ERA-Interim as well as other reanalysis datasets in representing surface climate characteristics of the Antarctic continent, particularly in the Antarctic Peninsula (e.g., Tetzner et al. 2019; Gossart et al. 2019; Liu et al. 2019; Bozkurt et al. 2020). For instance, Bozkurt et al. (2020) noted that on the leeward side of the central Peninsula, ERA5 exhibits a reduction in warm bias of mean annual near-surface temperature (+ 2.9 °C) compared to that in ERA-Interim (+ 5.4 °C) at the Larsen Ice Shelf station for the period 1995–2012. Similarly, in a recent study, using 30 manned meteorological and 26 automatic weather stations, Dong et al. (2020) showed that ERA5 has the best performance for the monthly

averaged wind speed magnitude and the interannual variability of the near-surface wind speed in Antarctica for the period 1980–2018.

In addition to these evaluations, we evaluated ERA5 temperature data with the available observation stations in the Antarctic Peninsula (see Fig. S1). It can be stated that ERA5 shows an overall good skill in capturing temperature variability and trends for most of the stations, except for a notable warm bias at the Larsen Ice Shelf station. Given that ERA5 captures reasonably well the temperature variability of the other leeward stations (Marambio and Butler Island), we suspect that ERA5 might have difficulties to capture snow pack properties at the surface of the Larsen Ice Shelf, which might be more pronounced during melt events. Similar issues were reported over the Greenland Ice Sheet (Delhasse et al. 2020). Due to the overall good match with observational temperature datasets, ERA5 can reasonably be considered as a reference.

2.2 Global and regional climate model simulations

We used daily and monthly mean temperature and precipitation obtained from 19 GCM simulations participating the CMIP5 (see Table S1 for the list of models). The dataset consists of one ensemble member (r1i1p1) from each CMIP5 model with a baseline period (1981–2005, ALL forcing historical) and near future period (2020–2044) under RCP8.5 scenario that corresponds to a future with no control policies of greenhouse gases.

We also performed high resolution RCM simulations using Polar Weather Research and Forecasting Model (Polar-WRF version 3.9.1) (Hines and Bromwich 2008; Bromwich et al. 2009; Hines et al. 2011) which is a polar-optimized version of the WRF model (Skamarock et al. 2008). The model includes modified land-surface model sea ice representation, allowing the specification of variable sea ice thickness, sea ice fraction and snow depth over sea ice. These modifications also include optimal values of snow thermal properties and improved heat flux calculations. The modeling experiment was conducted over the Antarctic Peninsula with two nested domains at 0.4° (~ 45 km) and 0.13° (~ 15 km) spatial resolutions on a polar stereographic projection (Fig. 1b). In this study, we used only high-resolution simulation results from the inner domain (d02, see Fig. 1b), which is centered on the Antarctic Peninsula and Larsen Ice Shelf, and has 208 × 190 grid cells. This domain employs 61 vertical levels between the surface and the model top at 10 hPa. More information about the model, simulation set up and physical configuration can be found in Bozkurt et al. (2020).

Polar-WRF was used to downscale global bias-corrected climate model output data from version 1 of National Center for Atmosphere Research's (NCAR) Community Earth System Model (CESM1) that participated in CMIP5. The reason for choosing NCAR-CESM1-CORRECTED (NC-CORR, hereafter) model outputs to force Polar-WRF (PWRF-NC-CORR, hereafter) for the baseline and near future periods was merely based on data availability and file format. Within this dataset, there was only one ensemble member (r6i1p1) available to drive the Polar-WRF model, belonging to Mother of All Runs (MOAR). Initial and boundary conditions for the historical simulations (1976–2005) and RCP8.5 scenario (2006–2044) were acquired from the https://rda.ucar.edu/datasets/ds316.1/. We used the same baseline period (1981–2005) and near future period (2020–2044) for the comparisons. The bias-corrected dataset (0.9° × 1.25° spatial resolution) consists of 26 pressure levels and contains all the variables needed for the initial and boundary conditions (6-h intervals) for PWRF simulations such as upper level fields (winds, geopotential heights, temperature, humidity) and surface variables (temperature, sea level pressure, winds). The variables were bias-corrected using the ECMWF Interim Reanalysis (ERA-Interim) fields for 1981–2005. The bias correction method corrects the mean state while retaining synoptic and climate scale variability. These bias-corrected variables do not include precipitation, therefore, we used precipitation from the raw NC simulations. More information about NC-CORR is available in Bruyére et al. (2015). A comparison of the bias-corrected NC-CORR with the raw NC shows that westerlies and MSLP are improved in the bias-corrected fields with a much closer pattern to those in ERA5 (see Fig. S2). Particularly, the raw NC exhibits unrealistically strong westerlies and deep low-pressure centers within the westerly belt (i.e., polar vortex).

In addition to Polar-WRF simulations, we used the Royal Netherlands Meteorological Institute (KNMI) Regional Atmospheric Climate Model (KNMI-RACM021P) model outputs forced with ICHEC-EC-EARTH (EC, hereafter, 1.1215 ° × 1.125° spatial resolution) (Hazeleger et al. 2008). RACMO simulations (RACMO-EC, hereafter) were performed by the KNMI and obtained from the Coordinated Regional Climate Downscaling Experiment (CORDEX) (Giorgi et al. 2009) dedicated to the Antarctic domain at 0.44° (~ 50 km) spatial resolution and 40 vertical levels. RACMO model (v2.1) was built on the ECMWF physics package (cycle CY23R4). The reason for choosing this simulation is merely based on the availability of data and the completeness of the simulations. More information about the model and its application on polar regions can be found in Van Meijgaard et al. (2008), Lenaerts et al. (2012) and Van Wessem et al. (2016).

A summary of the reanalysis and simulations used in this study is given in Table 1.

Table 1 List of the reanalysis and simulations used in this study

Source	Lateral boundary conditions	Resolution	Period
ERA5	–	0.25 ×0.25° (~ 30 km)	1981–2005
19 GCMs (CMIP5, r1i1p1)	–	Varying: interpolated to a common grid of 1.5 ×1.5° (~ 170 km)	1981–2005 2020–2044
RACMO21P (CORDEX)	EC-EARTH (r1i1p1)	0.44 ×0.44° (~ 50 km)	1981–2005 2020–2044
Polar-WRF	NCAR-CESM1-CORRECTED (r6i1p1)	0.13 ×0.13° (~ 15 km)	1981–2005 2020–2044

2.3 Methodology

Given the different climate characteristics at each side of the mountain barrier, we assessed the results dividing the Peninsula into windward and leeward sides (see Fig. 1a). We also defined a Larsen Ice Shelf area to focus on changes in melt and rain days. Shapefiles of windward and leeward regions as well as Larsen Ice Shelf were used for masking, and only grid points within the shapefiles were used for spatial-average comparisons. Due to the different spatial resolutions of the GCMs used in this study, all the models were interpolated onto a common grid of 1.5 ×1.5° using bilinear interpolation for temperature. In terms of precipitation, we used first order conservative remapping method that conserves the total area integral of the precipitation (Jones 1999). This technique is assumed to be appropriate for analysis of precipitation fluxes at different resolution grids (e.g., Di Luca et al. 2013; Guttler et al. 2015). The use of multimodel climate simulations has the advantage of providing an uncertainty range. For instance, the range of individual models are shown by the box-plot whiskers in the box plots and depict the maximum and minimum values of the individual CMIP5 models. With the same approach, the boxes in box plots correspond to the 25th and 75th percentiles of the individual CMIP5 models. This allows us to show the uncertainty range of the historical simulations and projections together with dynamically downscaled products. We focused on annual, summer (December–January–February, DJF), autumn (March–April–May, MAM), winter (June–July–August, JJA), spring (September–October–November, SON) and monthly time scales.

In addition, we calculated melt days that are defined as the days when near-surface temperature is above 0 °C for each simulation for the Larsen Ice Shelf. We also calculated rain days that are defined as the days when daily precipitation ≥ 1 mm on melt days. This calculation was performed by determining the days when near-surface temperature was above 0 °C for at least 50% of grids within the Larsen Ice Shelf. Then, the indices of these days were used to extract the rain days (≥ 1 mm) for at least 50% of grids within the Larsen Ice Shelf.

3 Results

3.1 Evaluation of the circulation patterns for historical simulations

Figure 2 shows spatial distribution of MSLP for 1981–2005 period obtained from ERA5, CMIP5 ensemble mean, EC, RACMO-EC, NC-CORR and PWRF-NC-CORR. Overall, both boundary conditions show similar MSLP patterns with ERA5 and CMIP5 ensemble mean (Fig. 2a–d). In particular, NC-CORR shows a very similar MSLP pattern with ERA5, and exhibits a slightly deeper MSLP over the Amundsen Sea than that in EC and CMIP5 (Fig. 2d). This is reasonable given the fact that NC-CORR was bias-corrected using the ECMWF ERA-Interim reanalysis fields. The Amundsen Sea sector shows a notable interannual variability in each product, however, NC-CORR yields a slightly larger interannual variability than other simulations as well as ERA5, since the bias correction method corrects only the mean state. Both dynamically downscaled simulations show a very similar synoptic pattern to that of their respective boundary conditions (Fig. 2e, f).

Given that the climate of the Antarctic Peninsula is known to be sensitive to the strength and position of the westerlies, we also compare representation of the westerly winds (850 hPa) in the boundary conditions with ERA5 and CMIP5 models (Fig. 3). EC and NC-CORR have a good representation of the westerlies with respect to ERA5. Nonetheless, NC-CORR represents the westerlies a little stronger with a slightly larger interannual variability compared to the other simulations and ERA5 (Fig. 3d). Regarding the position of the westerly winds maximum, ERA5 and NC-CORR show a very similar position of the westerly winds maximum (~ 52 °S) (Fig. 3e). CMIP5 ensemble mean and EC yield a bit more northern (~ 50 °S) and southern (~ 54 °S) position

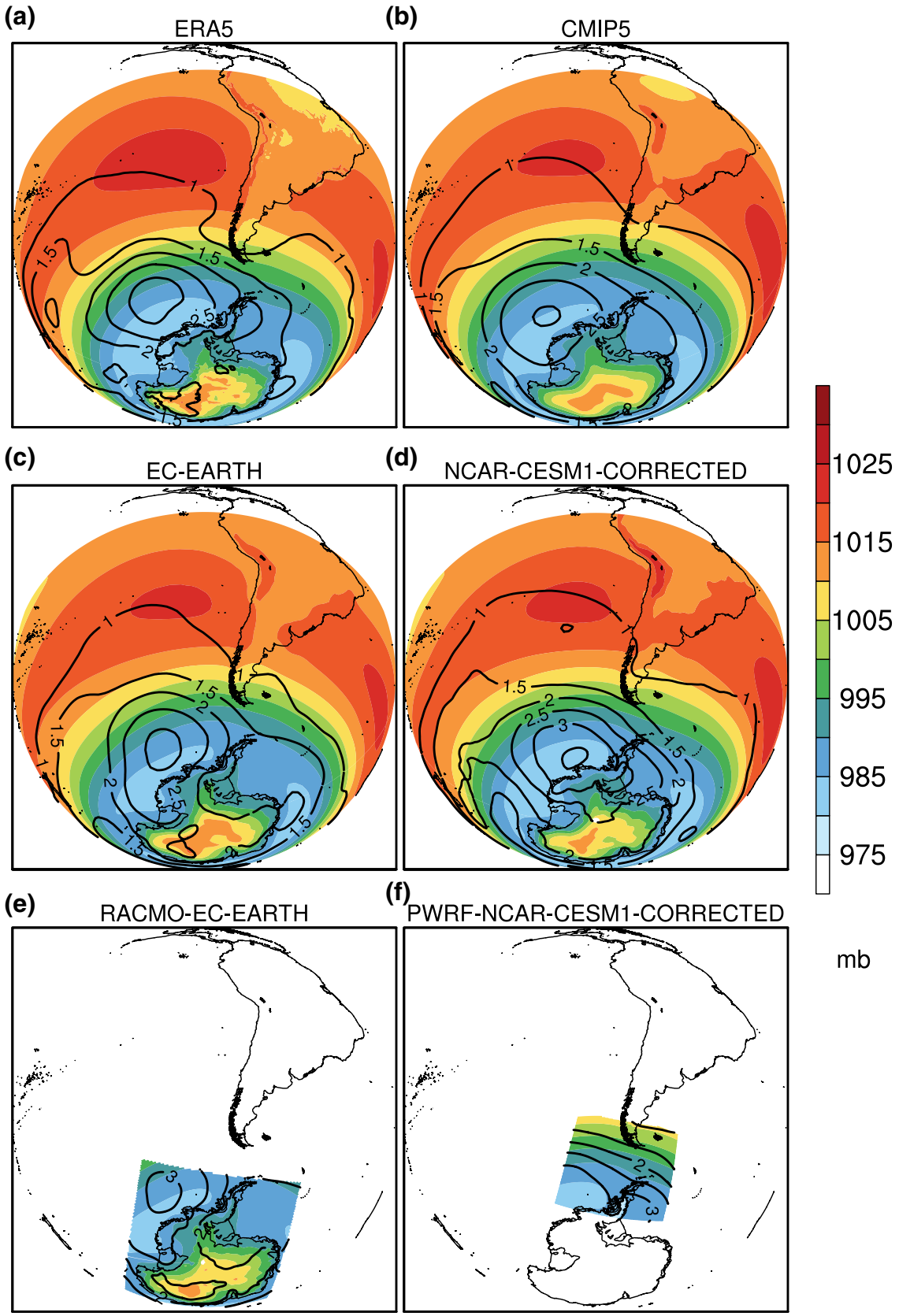
(a)
ERA5
(b)
CMIP5
(c)
EC-EARTH
(d)
NCAR-CESM1-CORRECTED
(e)
RACMO-EC-EARTH
(f)
PWRF-NCAR-CESM1-CORRECTED
1025
1015
1005
995
985
975
mb

◂**Fig. 2** **a** Spatial distribution of mean annual mean sea level pressure (shaded) for 1981–2005 period obtained from ERA5, **b** CMIP5 ensemble mean, **c** EC-EARTH, **d** NCAR-CESM1-CORRECTED, **e** RACMO-EC-EARTH and **f** PWRF-NCAR-CESM1-CORRECTED. Contour lines correspond to interannual variability, i.e., standard deviation of mean sea level pressure (contour lines at every 0.5 mb)

of the westerly winds maximum, respectively, compared to the ERA5 and NC-CORR.

Near-surface zonal wind climatology over the Antarctic Peninsula obtained from the boundary conditions and dynamically downscaled simulations indicates that both simulation pairs show very similar patterns of near-surface zonal winds (Fig. S3). Different from the boundary conditions, both RCMs, particularly PWRF-NC-CORR, yield stronger wind patterns on the leeward side, highlighting the potential role of the resolution and topography.

3.2 Projections

3.2.1 Circulation patterns

Figures 4 and 5 show projected mean annual changes in MSLP patterns and westerlies, respectively, for CMIP5 ensemble mean, boundary conditions and RCM outputs (only for MSLP pattern). Overall, CMIP5 ensemble mean shows deepening of low-pressure systems around the Antarctic continent and strengthening of anticyclonic conditions over the mid-to-higher latitudes accompanied with strengthening of the westerlies that are also shown by previous studies (Figs. 4a, 5a) (e.g., Bracegirdle et al. 2008; Zheng et al. 2013; Marshall et al. 2017; Screen et al. 2018). CMIP5 ensemble mean and EC yield a slight northern and southern shift of the position of the westerly winds maximum, respectively, while NC-CORR yields no change (not shown).

Interestingly, EC model depicts a notable deepening of the Amundsen Sea Low and strengthening of anticyclone over the southwest-southern South America (Fig. 4b). This pattern has been shown to trigger moisture transport and warm air advection from the lower latitudes towards the Antarctic Peninsula by means of atmospheric rivers (Bozkurt et al. 2018; Wille et al. 2019). On the other hand, NC-CORR shows an opposite pattern: decrease of the MSLP on both the windward and leeward sides of the Antarctic Peninsula and strengthening of anticyclonic conditions over the western sector of the Amundsen Sea (Fig. 4c). In addition, different from the EC and CMIP5 ensemble mean, NC-CORR shows weakening of the westerlies over a large part of the Peninsula, except the northernmost part (Fig. 5c). Both dynamically downscaled simulations show very similar projected changes to their driving models, indicating almost identical synoptic forcing in both GCMs and RCMs (Fig. 4d, e). However, PWRF-NC-CORR exhibits a slightly larger decrease of the MSLP compared to the its boundary conditions (Fig. 4e).

3.2.2 Temperature

Figure 6 shows the spatial pattern of projected changes in mean annual near-surface temperatures of CMIP5 ensemble, EC, RACMO-EC, NC-CORR, and PWRF-NC-CORR. It also shows differences between two RCMs and GCMs. Overall, temperatures are projected to increase by about 1.2–1.8 °C across the entire Peninsula in the CMIP5 ensemble mean under the RCP8.5 scenario (Fig. 6a). The CMIP5 ensemble mean projections show that leeward side of the Peninsula is projected to have slightly larger temperature increases than that on the windward side. This might be associated with the potential amplified warming coming from the regional-scale features largely dominated by sea-ice loss over the leeward side. In this respect, as shown by Turner et al. (2013) many of the CMIP5 models have important biases in capturing reference period sea-ice characteristics that can potentially affect the projected changes. For instance, Turner et al. (2013) highlighted that negative trends in Antarctic sea ice extent in most of the model runs over 1979–2005 are not consistent with the observed increase over the last 30 years.

EC model depicts larger temperature increases on the windward side especially over the Alexander Island (~ 1.8 to 2.4 °C) (Fig. 6b). As shown in the circulation pattern changes, a potential increase in moisture transport and warm air advection in EC model seems to be a reason for larger temperature increases on the windward side. RACMO-EC follows a pattern similar to its driving fields, nonetheless, some geographical variations are notable in the dynamically downscaled projections such as less warming on the leeward side, especially over the Larsen Ice Shelf and southwest windward side where EC has notable warming (Fig. 6c, d). This might also indicate that GCMs can have amplified warming over the areas where sea-ice is more prevalent.

The impact of the driving model on the RCM simulations is also dominant in the PWRF-NC-CORR (Fig. 6e, f). Similar to RACMO-EC, PWRF-NC-CORR also exhibits less temperature increases over the Larsen Ice Shelf and southwest windward side compared to the NC-CORR (Fig. 6f, g). Different from the EC and RACMO-EC paired projections, both NC-CORR and PWRF-NC-CORR project smaller temperature increases across the Peninsula (up to ~ 1.2 °C). It can be speculated that these differences are related to the weakening of the westerlies depicted in the NC-CORR (Fig. 5c) over a large part of the Antarctic Peninsula, which imply less southeastward advection of warm midlatitude air towards the windward side and therefore less adiabatic warming over the lee side.

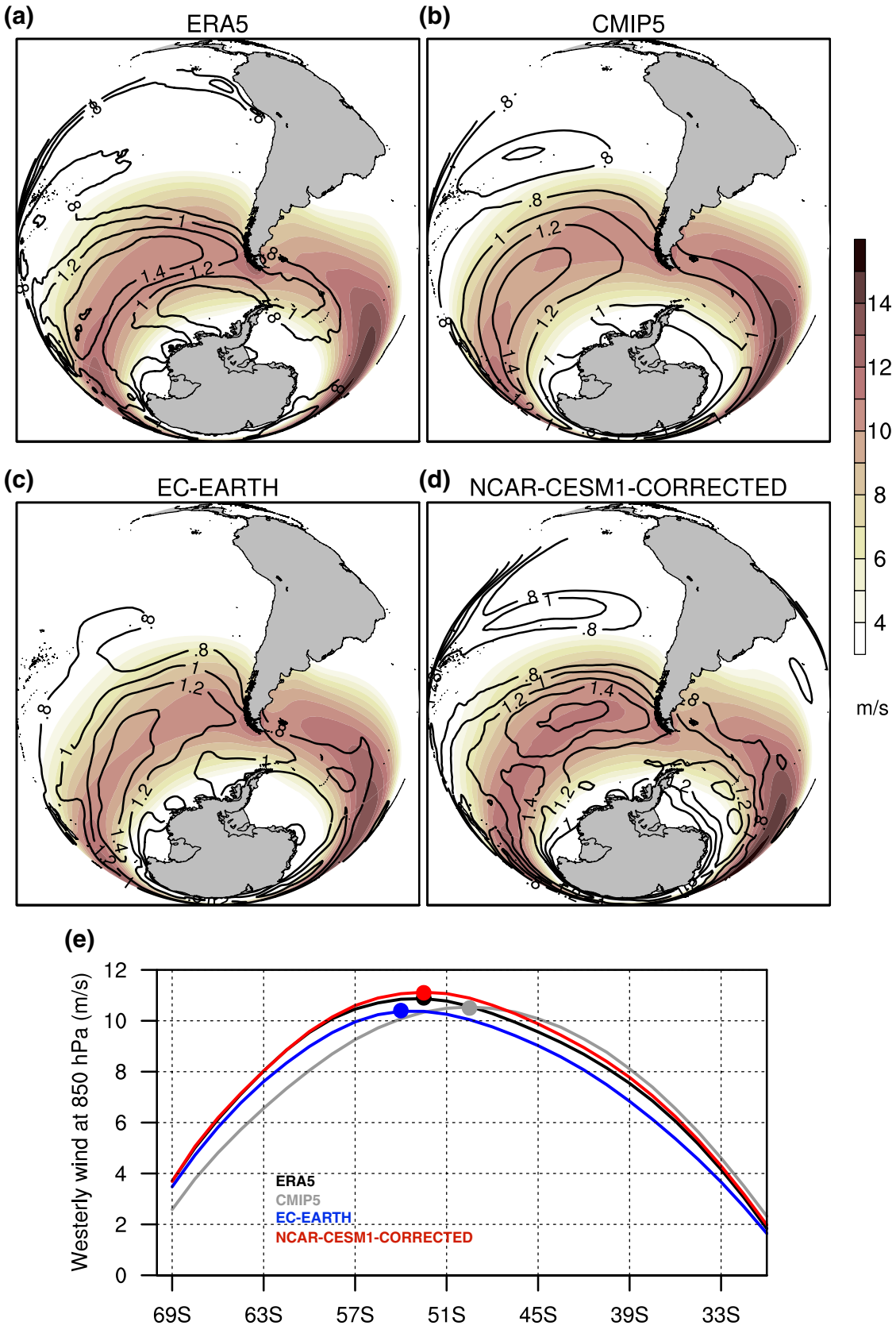
(a)
ERA5
(b)
CMIP5
(c)
EC-EARTH
(d)
NCAR-CESM1-CORRECTED
14
12
10
8
6
4
m/s
(e)
Westerly wind at 850 hPa (m/s)
12
10
8
6
4
2
0
69S
63S
57S
51S
45S
39S
33S
ERA5
CMIP5
EC-EARTH
NCAR-CESM1-CORRECTED

◂**Fig. 3** **a** Spatial distribution of mean annual 850 hPa zonal wind speed (shaded) for 1981–2005 period obtained from ERA5, **b** CMIP5 ensemble mean, **c** EC-EARTH and **d** NCAR-CESM1-CORRECTED. Contour lines correspond to interannual variability, i.e., standard deviation of 850 hPa zonal wind (contour lines at every 0.2 m s^{-1}). **e** Also shown is reference period mean annual zonal mean 850 hPa westerly climatology over the southern Southwest Pacific (120 W–80 W) obtained from ERA5 (black), CMIP5 ensemble mean (gray), EC-EARTH (blue) and NCAR-CESM1-CORRECTED (red). Markers correspond to the latitudes of maximum wind speed

In order to asses model uncertainties and to provide a context for future projections, Fig. 7 shows box plots of windward and leeward mean seasonal and annual near-surface temperatures for the periods of 1981–2005 (circle) and 2020–2044 (square) derived from the ERA5, CMIP5 models, EC, RACMO-EC, NC-CORR and PWRF-NC-CORR. On the windward side, the CMIP5 ensemble mean largely matches with the ERA5 in representing the climatology for DJF and MAM seasons (Fig. 7a). A large intermodel range on the windward side in JJA is notable. The EC model generally takes place in the upper limits of the CMIP5 models range, indicating a warmer reference period compared to the other simulations. Unlike the EC, RACMO-EC shows a closer near-surface climatology to ERA5, which can be associated with RCM physics since RACMO model was built on the ECMWF physics package.

PWRF-NC-CORR yields a colder climatology compared to NC-CORR, although they exhibit almost identical synoptic conditions (see Fig. 2). In particular, PWRF-NC-CORR yields relatively cold conditions over the windward side and Alexander Island (Fig. S4). We speculate that this can be related with the physical configuration of PWRF that can result in differences in radiative fluxes (e.g., King et al. 2015; Listowski and Lachlan-Cope 2017). Indeed, Bozkurt et al. (2020) noted a similar colder climatology depicted in PWRF simulations driven by ERA-Interim reanalysis when comparing with RACMO simulations driven by the same reanalysis. In the same study, Bozkurt et al. (2020) highlighted that there was a deficit in the surface downwelling longwave radiation in PWRF compared to the RACMO, which might explain colder climatology introduced by PWRF, particularly on the windward side.

CMIP5 ensemble mean for the near future (2020–2044) shows pronounced increases in MAM and JJA (+ 1.2 to + 2°C, respectively, see Table 2) on the windward side. The large intermodel range depicted in JJA for the historical period tends to persist in near future. Both RCMs show very close changes to those in the driving fields with less warming in NC-CORR and PWRF-NC-CORR compared to the other simulations, except for MAM (see Table 2).

On the leeward side, the CMIP5 ensemble mean generally yields colder conditions, except for MAM, with respect to ERA5 (Fig. 7b). A large intermodel range exists among the CMIP5 models in MAM and JJA. Regarding the driving fields, NC-CORR tends to have a slight warmer condition with respect to the ERA5 for the historical period. Dynamically downscaled simulations generally follow the driving fields in representing the climatology, nonetheless, some differences are notable such as the existence of relatively cold conditions in PWRF-NC-CORR in MAM and JJA. Near future period shows more notable temperature increases in the CMIP5 ensemble mean for MAM and JJA (+ 2 °C and + 2.1 °C, respectively, see Table 2). RACMO-EC generally indicates smaller temperature increases with respect to EC. PWRF-NC-CORR follows closely with NC-CORR except during JJA where NC-CORR shows a cooling signal relative to historical period (see Table 2).

A more detailed analysis of the temperature projections can be obtained by looking at the annual cycle (Fig. 8). Overall, mean annual cycle climatology depicted in both RCMs follows closely those of the driving fields on both windward and leeward sides, except colder conditions in PWRF-NC-CORR with respect to NC-CORR in cold season months. Regarding the projected temperature changes, both driving fields and dynamically downscaled simulations yield very similar changes on both sides. On the windward side, NC-CORR and PWRF-NC-CORR show the largest increase in temperature in May (+ 3 °C and + 3.5 °C, respectively), whereas EC and RACMO-EC indicate the largest temperature increase in July (~ + 2.5 °C) (Fig. 8b). Unlike the EC and RACMO-EC, NC-CORR and PWRF-NC-CORR project a decrease in temperature in August.

On the leeward side, projected temperature changes derived from the CMIP5, RACMO-EC, and RACMO-EC EARTH simulations range from + 0.5 to + 2.1 °C (Fig. 8d). On the other hand, NC-CORR and PWRF-NC-CORR largely differ from the other simulations from June to October with some temperature decreases. It can be speculated that, as shown before, a dipole-like pattern characterized by a decrease in MSLP over the northeast Peninsula and a notable weakening of the Amundsen Sea Low, might lead to weakening of the westerlies over the Antarctic Peninsula, and thus a prevailing colder continental climate in the winter season (see Fig. S5). A slightly larger warming in PWRF-NC-CORR with respect to NC-CORR can be shaped by the RCM microphysics associated with the relatively cold historical period climatology during the cold season, and thus, resulting in a larger warming rates in the projections.

3.2.3 Precipitation

Figure 9 presents the spatial pattern of projected relative changes in annual total precipitation in near future compared to the historical period. According to the CMIP5 ensemble mean, precipitation is projected to increase by ~ +5% across

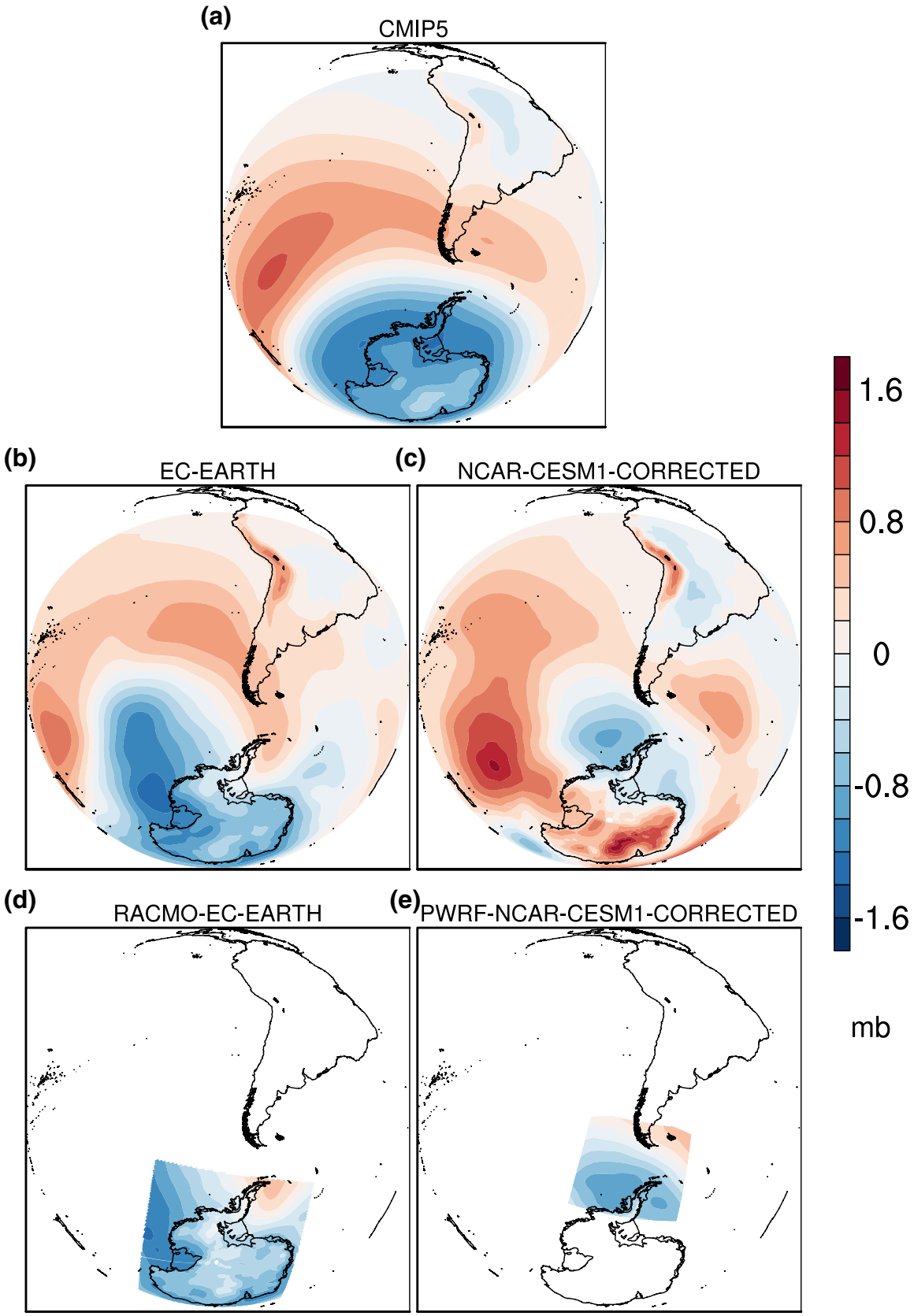
(a)
CMIP5
(b)
EC-EARTH
(c)
NCAR-CESM1-CORRECTED
(d)
RACMO-EC-EARTH
(e)
PWRF-NCAR-CESM1-CORRECTED
1.6
0.8
0
-0.8
-1.6
mb

◂**Fig. 4** **a** Projected mean annual mean sea level pressure changes for 2020–2044 period (under RCP8.5) with respect to 1981–2005 period obtained from CMIP5 ensemble mean, **b** EC-EARTH, **c** NCAR-CESM1-CORRECTED, **d** RACMO-EC-EARTH and **e** PWRF-NCAR-CESM1-CORRECTED

the entire Peninsula (Fig. 9a). EC projects a pronounced precipitation increase over the southwestern part of the Peninsula, particularly around the Alexander Island (~ + 10 to + 15%), whereas a smaller precipitation increase is projected on the leeward side (~< + 5%). It even projects a slight decrease of precipitation over the southern parts of the leeward side. Following this signal, RACMO-EC gives a similar spatial pattern of precipitation change on the windward side, nonetheless it shows larger increases (~ + 12 to + 20%), highlighting the role of a finer detailed topography and orographic influences, which is more pronounced in DJF. Although mean windward precipitation increase is also relatively large in SON (see Table 3), seasonal spatial precipitation changes highlight a more pronounced orographic barrier influence (i.e., a more increase in precipitation confined to the cordillera) in DJF (not shown).

A notable difference between the EC and RACMO-EC takes place on the leeward side where RACMO-EC mostly indicates decreases in precipitation (up to ~ − 10%). This projected decrease in precipitation on the leeward side is more pronounced in DJF and MAM (Fig. S6, see also Table 3). On the other hand, in these seasons, RACMO-EC shows almost the same areas of the precipitation decreases with those in EC indicating the inherited influences of the boundary conditions on the RCM results. Nonetheless, RACMO-EC yields a more pronounced decrease in precipitation over these areas, which can be associated with the RCM physics. Yet, although finer-scale features (i.e., precipitation shadow) on the eastern side of the Antarctic Peninsula are not captured at 55 km resolution RACMO simulations (Van Den Broeke and Van Lipzig 2004; Van Lipzig et al. 2008), RACMO model can represent better the barrier effect of the topography compared to the coarse-resolution driving field, which can also result in more pronounced decrease in precipitation on the leeward side.

NC and PWRF-NC-CORR project similar spatial pattern of increases in precipitation over the northern Peninsula (~ + 5 to + 10%), however, unlike the NC, PWRF-NC-CORR

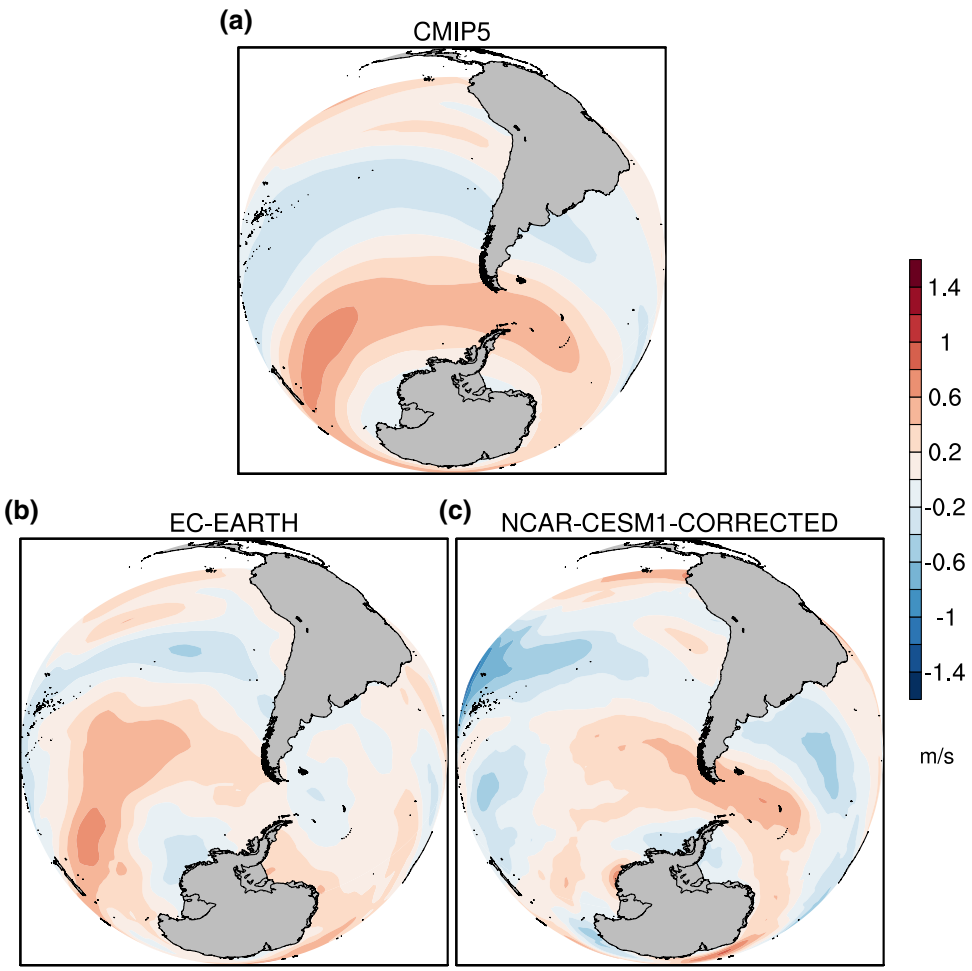

Fig. 5 **a** Projected mean annual 850 hPa zonal wind speed changes for 2020–2044 period (under RCP8.5) with respect to 1981–2005 period obtained from CMIP5 ensemble mean, **b** EC-EARTH, **c** NCAR-CESM1-CORRECTED

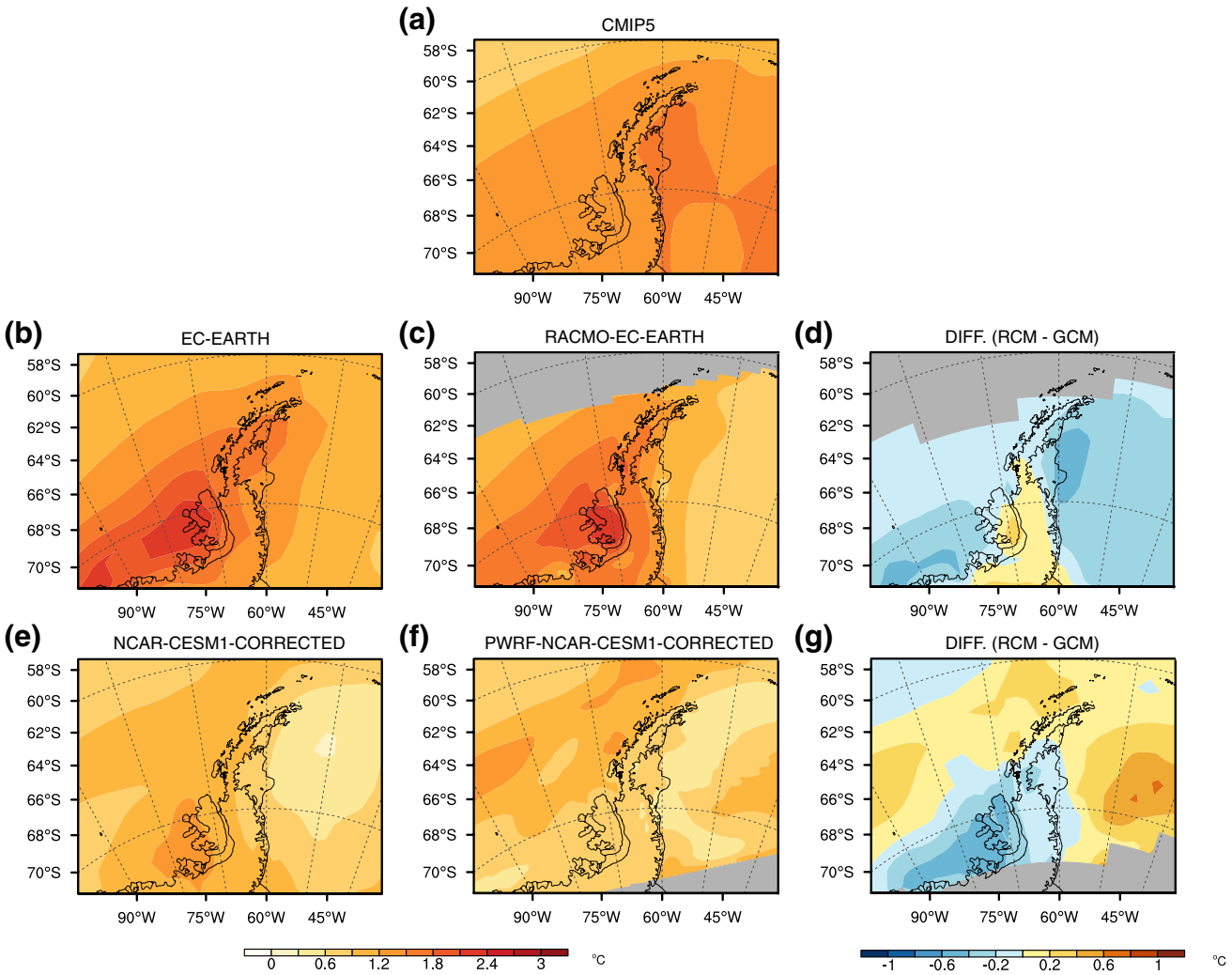

Fig. 6 **a** Projected mean annual near-surface temperature differences for 2020–2044 period (under RCP8.5) with respect to 1981–2005 period obtained from CMIP5 ensemble mean, **b** EC-EARTH, **c** RACMO-EC-EARTH, **d** differences between RACMO-EC-EARTH and EC-EARTH, **e** NCAR-CESM1-CORRECTED, **f** PWRF-NCAR-CESM1-CORRECTED and **g** differences between PWRF-NCAR-CESM1-CORRECTED and NCAR-CESM1-CORRECTED

indicates a decrease in precipitation (~ − 5%) over the central-southern parts of the inland territory of the Peninsula. This projected decrease in PWRF-NC-CORR might be more tied to microphysics schemes and a finer detailed topography as it coincides with the maximum of the topography over the central-southern parts of the inland territory of the Antarctic Peninsula (Fig. S7).

Regarding the monthly changes, both RACMO-EC and PWRF-NC-CORR match very closely with their boundary conditions, though RACMO-EC tends to exhibit slightly larger changes than EC on the windward side (Fig. 10a). RACMO-EC and EC have the largest precipitation increases in January (~ + 25% and + 18%, respectively), whereas PWRF-NC-CORR and NC show the largest precipitation increases in May (~ + 20% and + 23%, respectively), in which the CMIP5 ensemble mean has the largest precipitation increase too (~ + 10%). Similar to windward side, near future projections illustrate that RCMs largely follow the boundary conditions in each month for the leeward side (Fig. 10b). Nonetheless, RACMO-EC almost systematically yields lower changes with respect to the boundary conditions, a difference that is more pronounced in summer and autumn seasons (also shown in Fig. S6). PWRF-NC-CORR depicts a more increase in precipitation in October (~ + 30%) compared to NC (~ + 15%).

We close this subsection with bivariate climate change signal of mean annual temperature and total precipitation changes on the windward and leeward sides derived from the all simulations (Fig. 11). On the windward side, all CMIP5 simulations exhibit temperature increases (~ + 0.1 to + 2.5 °C) accompanied with precipitation increases (~ + 1 to + 13%) (Fig. 11a). Both NC-CORR and EC projections are

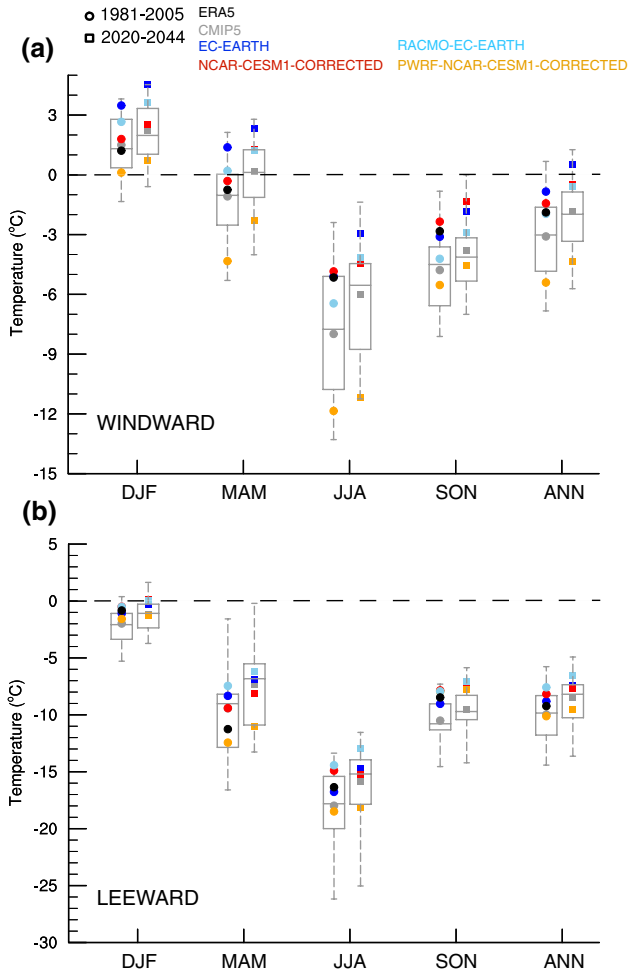

Fig. 7 **a** Box plots of windward mean seasonal and annual temperatures for the periods of 1981–2005 (circle) and 2020–2044 (square). Black and gray colors correspond to ERA5 and CMIP5 ensemble mean, respectively. The CMIP5 ensemble median is represented by the bar across the box and the box-plot whiskers represent the maximum and minimum values of the individual CMIP5 models. The box represents the 25th and 75th percentiles of the individual CMIP5 models. Blue and light blue colors correspond to EC-EARTH and RACMO-EC-EARTH, respectively. Red and orange colors correspond to NCAR-CESM1-CORRECTED and PWRF-NCAR-CESM1-CORRECTED, respectively. **b** Same as **a** but for the leeward side. Note that due to the large temperature differences, the axis values and intervals are not the same for the windward and leeward sides. Note the overlaps between the points (e.g., NCAR-CESM1-CORRECTED and CMIP5 ensemble mean on the leeward side for MAM)

very close to the CMIP5 ensemble mean changes. RACMO-EC slightly increases the temperature and precipitation changes compared to the EC, whereas PWRF-NC-CORR slightly increases temperature changes and reduces precipitation changes compared to the NC-CORR.

On the leeward side, projected changes in the CMIP5 ensemble mean are very close to those on the windward side (Fig. 11b). Regarding the GCM and RCM comparison, the most notable difference exists between RACMO-EC and EC where RACMO-EC reduces the temperature change and shows an opposite sign of precipitation change to that of the EC, indicating the influence of the amplified decrease signal detected in DJF and MAM on the annual scale. PWRF-NC-CORR yields very close projected changes to NC-CORR on the leeward side.

The sensitivity of precipitation increase to warming is $4.8\%K^{-1}$ for CMIP5 ensemble mean on the windward side. RACMO-EC and PWRF-NC-CORR show almost the same sensitivity values ($\sim 5\%K^{-1}$) with larger and lower values than their boundary conditions, respectively. As also indicated by Palerme et al. (2017), the sensitivity of precipitation increase to warming is expected to be much larger in Antarctica compared to the global mean, particularly by the end of the century. On the other hand, on the leeward side, simulations show less sensitivity values even negative sign (RACMO-EC), except NC-CORR and PWRF-NC-CORR which exhibit notably larger values ($\sim 9\%K^{-1}$). These inconsistencies on the leeward side indicate that there are still considerable uncertainties of temperature and precipitation projections for the Antarctic Peninsula.

3.2.4 Melt days and rain days

Figure 12 presents projected changes in mean annual melt days for CMIP5 ensemble mean, boundary conditions and RCMs. Overall, CMIP5 ensemble mean shows that northernmost part of the Antarctic Peninsula is projected to have the largest increases (~ 20 days per year), whereas Larsen Ice Shelf shows increases between ~ 4 and 12 days per year (Fig. 12a). Similar patterns are depicted in both boundary conditions, nonetheless, with more pronounced increases particularly on the windward side and Larsen Ice Shelf (Fig. 12b, d). Both RCM simulations show their largest increase over the northernmost part of the Antarctic Peninsula (Fig. 12c, e), and different from their driving fields, they show less increase in melt days, which is more prominent in the Larsen Ice Shelf.

Figure 13 shows box plots of mean annual number of melt days changes in the Larsen Ice Shelf. As depicted in spatial map plot, RCMs project a smaller increase in the number of melt days per year (8 days for RACMO-EC and 5 days for PWRF-NC-CORR) compared to their boundary conditions (Fig. 13a). CMIP5 ensemble mean shows an increase in melt days (~ 7 days per year), which is close to that in RCMs. Regarding the relative changes, RCMs project an increase by about 50% (RACMO-EC) and 40% (PWRF-NC-CORR). Interestingly, EC-EARTH shows a larger increase (~ 75%) while NC-CORR has a smaller increase (~ 25%) in relative changes. As noted by Bozkurt et al. (2020), ERA-Interim has some considerable biases in capturing recent temperature trends particularly over the Larsen Ice Shelf with a notable warm bias compared to the observations. Therefore, we

Table 2 Mean seasonal and annual temperature changes (°C) on the windward side from CMIP5 ensemble mean, boundary conditions and regional climate model simulations in near future (2020–2044) with respect to 1981–2005 period

Temperature change (°C)	DJF	MAM	JJA	SON	ANN
CMIP5 (Ensemble)	+ 0.7 (+ 0.8)	+ 1.2 (+ 2)	+ 2 (+ 2.1)	+ 0.9 (+ 0.9)	+ 1.2 (+ 1.5)
EC-EARTH	+ 1 (+ 0.8)	+ 0.9 (+ 1.4)	+ 2.1 (+ 2)	+ 1.3 (+ 1.3)	+ 1.3 (+ 1.4)
NCAR-CESM1-CORRECTED	+ 0.7 (+ 0.6)	+ 1.6 (+ 1.2)	+ 0.4 (− 0.3)	+ 1 (+ 0.3)	+ 0.9 (+ 0.5)
RACMO-EC-EARTH	+ 0.9 (+ 0.5)	+ 1 (+ 1.3)	+ 2.3 (+ 1.5)	+ 1.3 (+ 0.8)	+ 1.4 (+ 1)
PWRF-NCAR-CESM1-CORRECTED	+ 0.6 (+ 0.3)	+ 2 (+ 1.4)	+ 0.7 (+ 0.4)	+ 0.9 (+ 0.2)	+ 1.1 (+ 0.6)

Changes on the leeward side are presented in parentheses

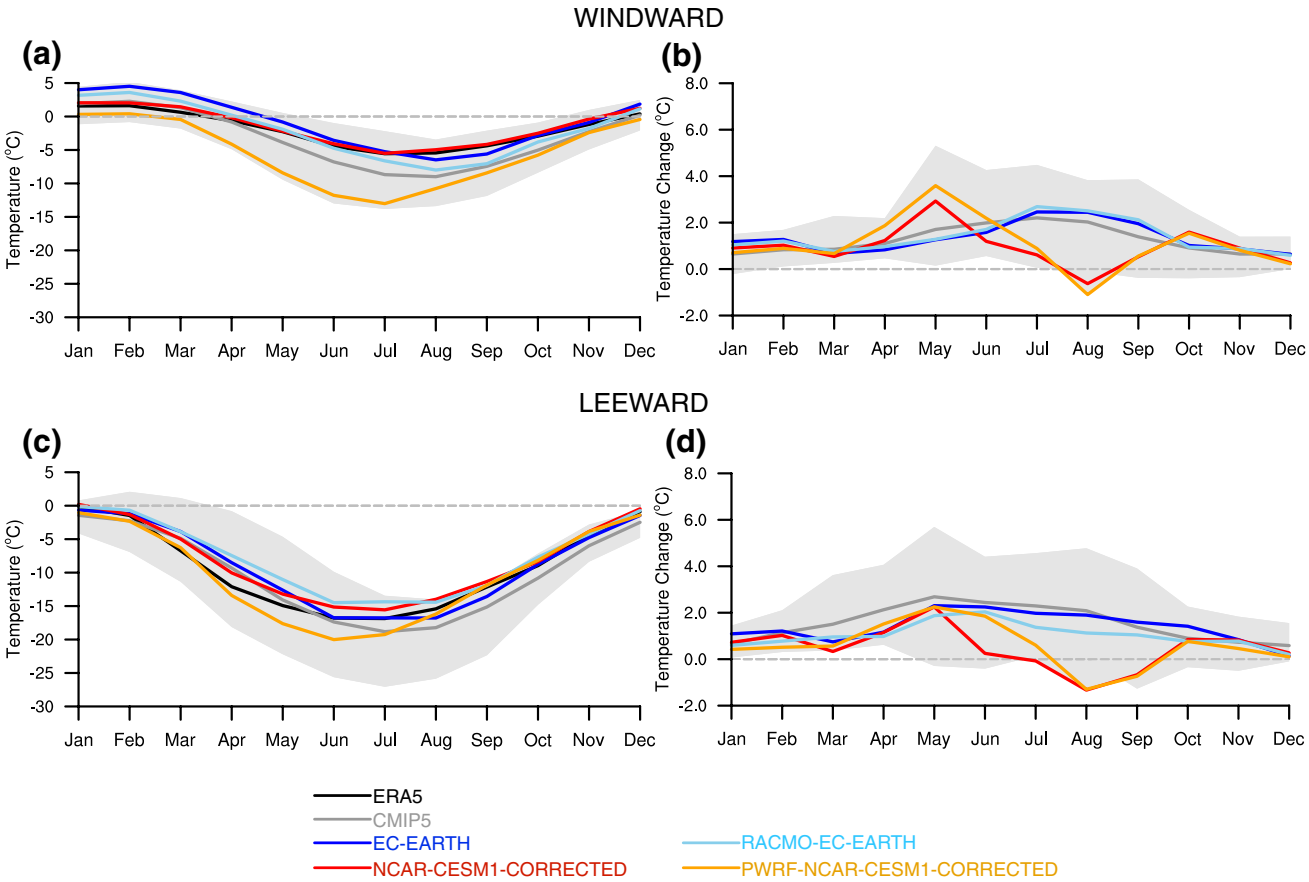

Fig. 8 **a** Reference period (1981–2005) windward mean annual cycle of near-surface temperature and **b**) absolute changes of near-surface temperature under RCP8.5 in near future (2020–2044). Black and gray lines correspond to ERA5 and CMIP5 ensemble mean, respectively. Blue and light blue lines correspond to EC-EARTH and RACMO-EC-EARTH, respectively. Red and orange lines correspond to NCAR-CESM1-CORRECTED and PWRF-NCAR-CESM1-CORRECTED, respectively. Shading shows the range of individual models of the CMIP5. **c**, **d** Same as **a**, **b** but for the leeward side, respectively

suspect that as NC-CORR uses ERA-Interim for bias correction, it somehow inherited this warm bias, which can be reflected in the melt days projections.

Finally, we present the same analysis of Fig. 13 but for rain days (Fig. 14). Each simulation indicates an increase of rain days. EC and NC-CORR show larger increases per year (~ 8.5 and 10.5 days, respectively) than CMIP5 ensemble

Fig. 9 **a** Projected mean annual precipitation differences for 2020–2044 period (under RCP8.5) with respect to 1981–2005 period obtained from CMIP5 ensemble mean, **b** EC-EARTH, **c** RACMO-EC-EARTH, **d** NCAR-CESM1 and **e** PWRF-NCAR-CESM1-CORRECTED. Note that bias-corrected boundary conditions of NCAR-CESM1 do not include precipitation, therefore, we use raw NCAR-CESM1 precipitation for the comparisons

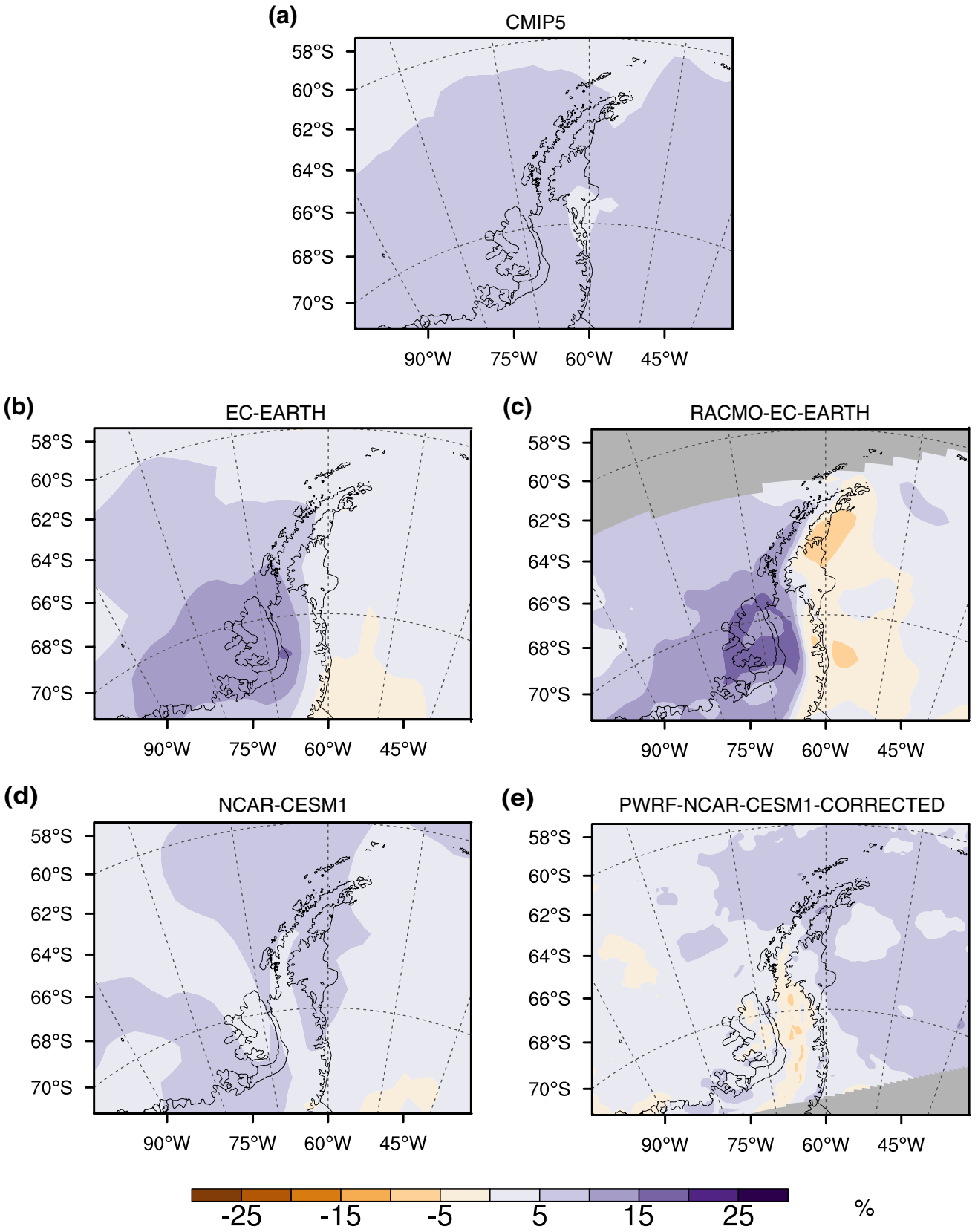
(a)
CMIP5
(b)
EC-EARTH
(c)
RACMO-EC-EARTH
(d)
NCAR-CESM1
(e)
PWRF-NCAR-CESM1-CORRECTED
58°S
60°S
62°S
64°S
66°S
68°S
70°S
90°W
75°W
60°W
45°W
-25
-15
-5
5
15
25
%

Table 3 Mean seasonal and annual precipitation changes (%) on the windward side from CMIP5 ensemble mean, boundary conditions and regional climate model simulations in near future (2020–2044) with respect to 1981–2005 period

Precipitation change (%)	DJF	MAM	JJA	SON	ANN
CMIP5 (Ensemble)	+ 5.5 (+ 5.5)	+ 7 (+ 5.9)	+ 6.6 (+ 7.3)	+ 3.3 (+ 3.9)	+ 5.7 (+ 5.6)
EC-EARTH	+ 5.1 (+ 3.1)	+ 1 (− 3.7)	+ 4.9 (+ 5.6)	+ 9.7 (+ 5.6)	+ 5.1 (+ 2.4)
NCAR-CESM1	+ 11.7 (+ 6.8)	+ 5.6 (+ 2)	+ 1.3 (+ 4.6)	+ 9.2 (+ 6.8)	+ 6.8 (+ 4.8)
RACMO-EC-EARTH	+ 10.3 (− 0.5)	+ 4.6 (− 8.7)	+ 3.9 (+ 3.3)	+ 10.5 (+ 4.3)	+ 7.1 (− 1.2)
PWRF-NCAR-CESM1-CORRECTED	+ 11.2 (+ 7.9)	+ 4.6 (+ 1.8)	+ 0.4 (+ 4.6)	+ 7.9 (+ 8.8)	+ 5.7 (+ 5.5)

Changes on the leeward side are presented in parentheses. Note that bias-corrected boundary conditions of NCAR-CESM1 do not include precipitation, therefore, we use raw NCAR-CESM1 precipitation for the comparisons

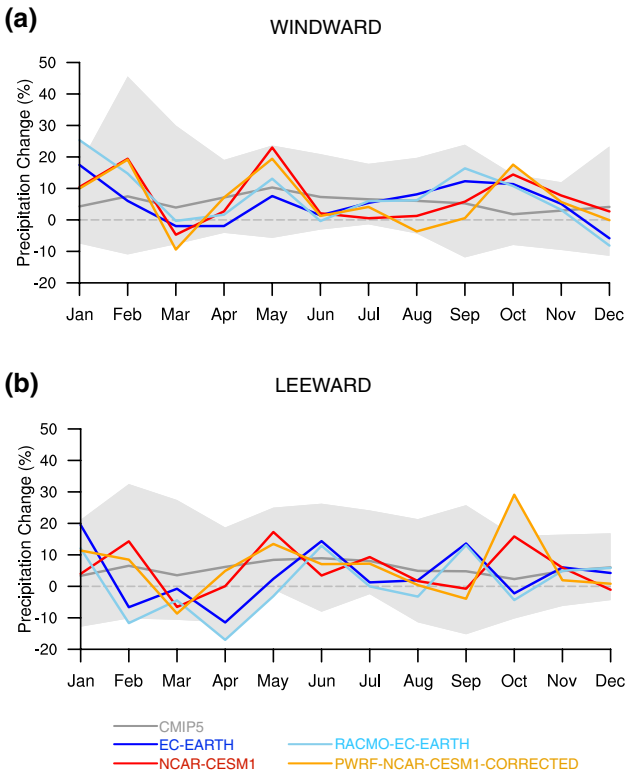

Fig. 10 **a** Windward mean relative precipitation changes under RCP8.5 in near future (2020–2044) with respect to reference period (1981–2005). Gray line corresponds to CMIP5 ensemble mean. Blue and light blue lines correspond to EC-EARTH and RACMO-EC-EARTH, respectively. Red and orange lines correspond to NCAR-CESM1 and PWRF-NCAR-CESM1-CORRECTED, respectively. Shading shows the range of individual models of the CMIP5. Note that bias-corrected boundary conditions of NCAR-CESM1 do not include precipitation, therefore, we use raw NCAR-CESM1 precipitation for the comparisons. **b** Same as **a** but for the leeward side

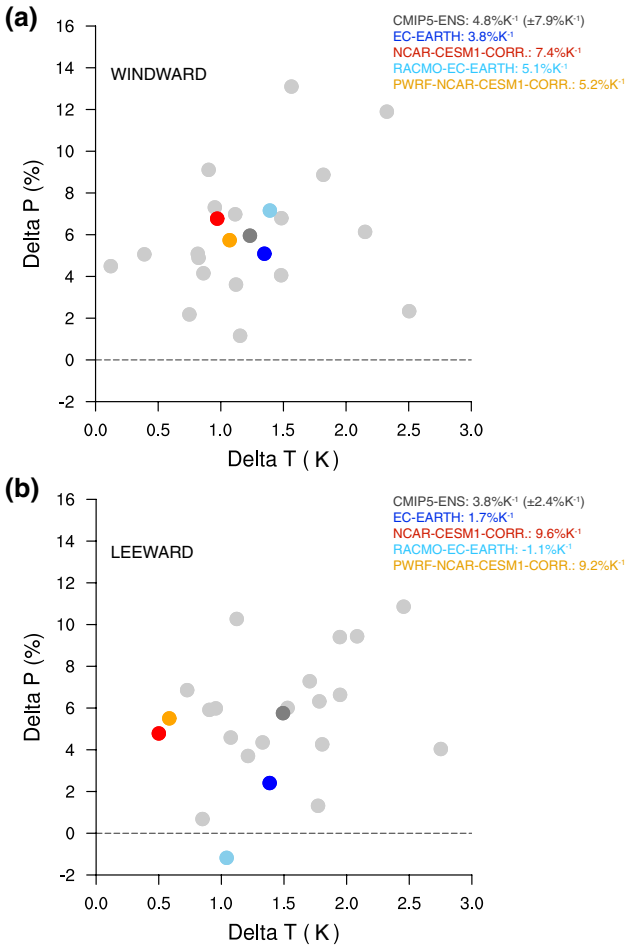

Fig. 11 **a** Projected windward mean annual temperature and precipitation differences for 2020–2044 period (under RCP8.5) with respect to 1981–2005 reference period. Gray color corresponds to CMIP5 models and dark gray color shows the ensemble mean. Blue and light blue colors correspond to EC-EARTH and RACMO-EC-EARTH, respectively. Red and orange colors correspond to NCAR-CESM1-CORRECTED and PWRF-NCAR-CESM1-CORRECTED, respectively. **b** Same as **a** but for the leeward side. Note that bias-corrected boundary conditions of NCAR-CESM1 do not include precipitation, therefore, we use raw NCAR-CESM1 output for precipitation. The legend also includes the sensitivity of precipitation increase to warming (in $\%K^{-1}$) for CMIP5 ensemble mean (plus/minus standard deviation of the individual models), EC-EARTH, RACMO-EC-EARTH, NCAR-CESM1-CORRECTED and PWRF-NCAR-CESM1-CORRECTED

mean (~ 5.5 days) and RCMs (~ 3 days). On the other hand, regarding the relative changes, CMIP5 ensemble mean shows an increase by around 90%, which seems to imply that the CMIP5 ensemble mean has too few melt days during the historical period. RCM simulations project an increase by about 40% (RACMO-EC) and 70% (PWRF-NC-CORR). A pronounced projected decrease in precipitation over the

Larsen Ice Shelf in RACMO-EC might be the reason for a smaller increase in rain days compared to EC. Relatively high rain day climatology for the reference period in NC-CORR yields a smaller increase of relative changes (~ 30%) compared to the other simulations.

4 Discussion

Based on the projection results presented in this study, it can be stated that CMIP5 models generally tend to have important uncertainties of the temperature increases, particularly over the leeward side of the Antarctic Peninsula. Given the influence by strong westerlies, mid-latitude baroclinic systems and moisture transport from the tropics, the complex interplay between important large-scale features such as SAM and ENSO tends to be a major source of uncertainty of the future climate projections. On one hand, a recent trend toward the positive phase of the SAM is projected to continue into the future, resulting in intensification of the westerlies and more warm moisture-laden air masses over the Antarctic Peninsula and other coastal areas (e.g., Bracegirdle et al. 2008; Zheng et al. 2013; Marshall et al. 2017; Screen et al. 2018). On the other hand, regional weather and climate variability of the Antarctic Peninsula is also tied to large-scale meridional forcing that is largely controlled by Rossby-wave dynamics generated by the tropical SST variability at different time scales from intraseasonal (e.g., Rondanelli et al. 2019) to decadal (e.g., Grassi et al. 2006). In this respect, previous studies pointed out the greater uncertainty in climate change projections of West Antarctica due to the inadequate representation of tropical and polar teleconnections (e.g., Ding et al. 2011; Abram et al. 2014; Hosking et al. 2016; Marshall et al. 2017).

Indeed, for instance, pronounced warming in the EC simulation seems to be shaped by the deepening of the Amundsen Sea Low and strengthening of anticyclone over the southwest-southern South America, which can potentially trigger atmospheric rivers and warm air advection from the low latitudes (e.g., Bozkurt et al. 2018; Wille et al. 2019; Rondanelli et al. 2019). On the other hand, weakening of the Amundsen Sea Low and more cyclonic conditions around the Antarctic peninsula in NC-CORR simulation seem to hinder westerlies, and thus, prevent warm air advection and moisture transport towards the Antarctic Peninsula, leading to smaller temperature increases in NC-CORR. This seems to be a possible continuation of short term natural interdecadal variability that still in the foreground. In this respect, previous studies highlighted the important role of natural variability and decadal changes in leading to recent cooling period (~ 1990s to 2015) over the Antarctic Peninsula (e.g., Carrasco 2013; Turner et al. 2016; Oliva et al. 2017). In particular, Turner et al. (2016) showed that more cyclonic conditions in the northern Weddell Sea shaped by the natural interdecadal variability are associated with the recent cooling trend over the Antarctic Peninsula.

Beside from large- and synoptic-scale forcing, CMIP5 models can have additional warming coming from the regional-scale features largely dominated by sea-ice loss particularly over the leeward side as many of the CMIP5 models have important uncertainties in representing sea-ice (Turner et al. 2013). These potential uncertainties at different spatial scales can result in different warming trends in the CMIP5 models not only for the observation period (e.g., Jones et al. 2019) but also for future projections. For instance, sea-ice extent with less than the "reality" for the reference period depicted in the CMIP5 models might tend to decrease anomalously under the warming conditions in the near future, leading to amplified regional warming over the areas where sea-ice is more prevalent such as leeward side. In this respect, sea-ice behavior complicates temperature projections over the Antarctic Peninsula. Indeed, large inconsistencies on the leeward side indicate that there are still considerable uncertainties of temperature and precipitation projections for the Antarctic Peninsula, highlighting the difficulties of achieving high quality and consistent projections from GCMs for the Antarctic Peninsula.

Regarding the RCM projections, we argue that RCMs are closely tied to the GCM fields since dominant and common changes from the boundary conditions are largely evident in the RCM simulations. This is consistent with previous studies that highlight the important role of the selection of GCM in shaping the RCM projections (e.g., Wilby et al. 2004; Graham et al. 2007; Niu et al. 2015; Addor et al. 2016). In particular, Liang et al. (2008) highlighted that a major portion of the present climate biases (either for RCM and GCM) are systematically propagated into future climate projections at regional scales. Nonetheless, we also note some interesting differences in projected temperature and precipitation fields between GCM and RCM simulations. Given that synoptic conditions in the RCMs are very similar to those in their boundary conditions, the added value of RCM projections can be found by the finer spatial detail at local-scale which can be associated with the RCM topography and physics. However, Sørland et al. (2018) highlighted that the capability of the RCMs to modify the climate change signals of the driving GCMs can even exist on scales that are considered well resolved by the driving GCMs. In our study, we highlight that these GCM and RCM differences might make more sense at local-scale such as Larsen Ice Shelf, particularly for melt days and rain days.

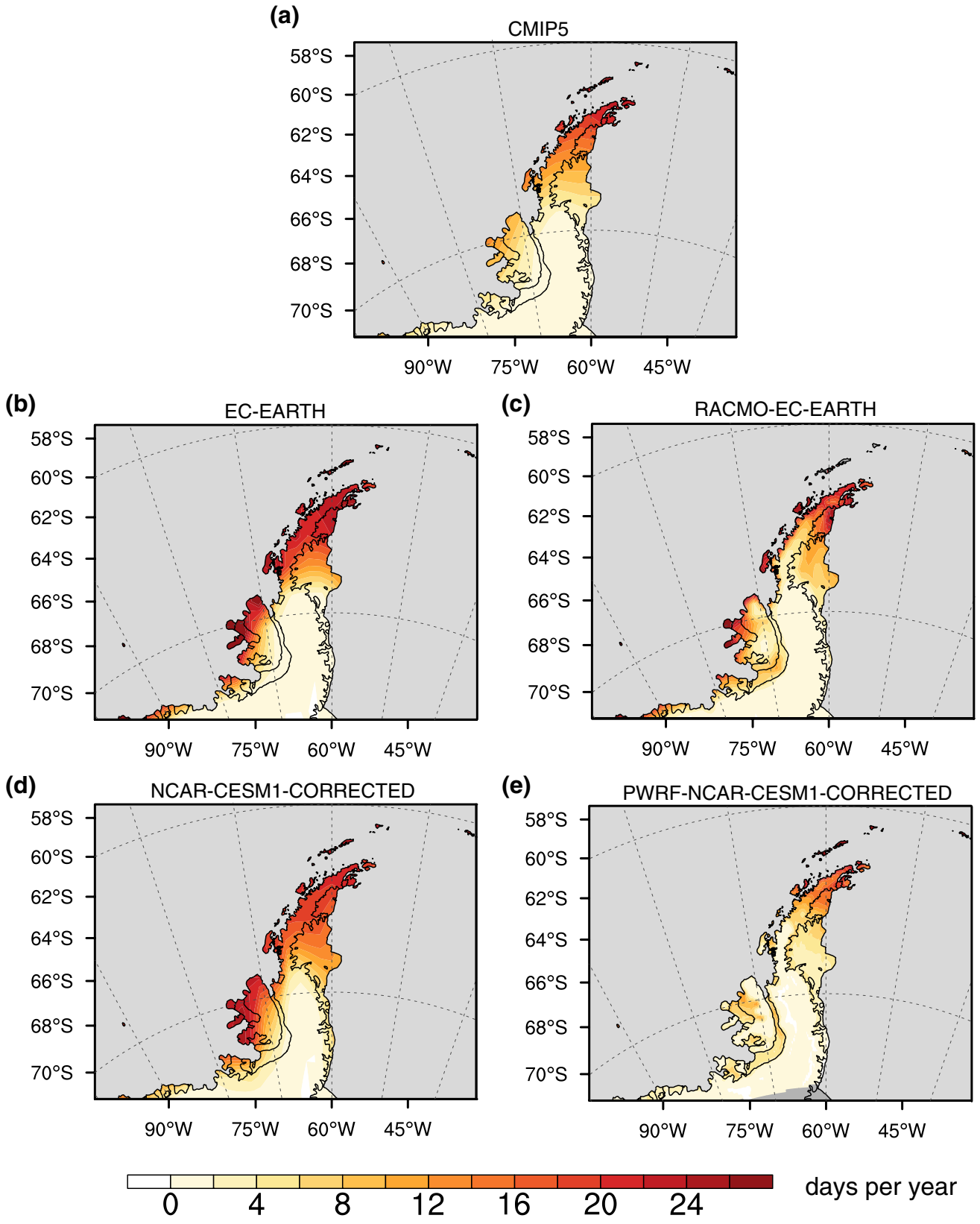

Fig. 12 **a** Projected mean annual number of melt days differences for 2020–2044 period (under RCP8.5) with respect to 1981–2005 period obtained from CMIP5 ensemble mean, **b** EC-EARTH, **c** RACMO-EC-EARTH, **d** NCAR-CESM1-CORRECTED and **e** PWRF-NCAR-CESM1-CORRECTED. Melt days are defined as the days when near-surface temperature is above 0 °C

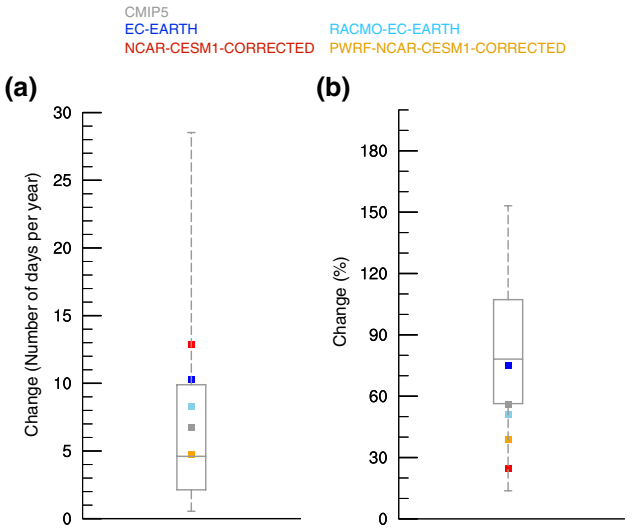

Fig. 13 **a** Box plot of absolute mean annual melt days changes for Larsen Ice Shelf. Gray color corresponds to CMIP5 ensemble mean. Blue and light blue colors correspond to EC-EARTH and RACMO-EC-EARTH, respectively. Red and orange colors correspond to NCAR-CESM1-CORRECTED and PWRF-NCAR-CESM1-CORRECTED, respectively. The CMIP5 ensemble median is represented by the bar across the box and the box-plot whiskers represent the maximum and minimum values of the individual CMIP5 models. The box represents the 25th and 75th percentiles of the individual CMIP5 models. **b** Same as **a** but for relative changes %. Note that five of the CMIP5 models were excluded in the relative changes plot as they have too few melt days per year for the reference period (i.e., melt days per year < 2 days) resulting in anomalously high projection values

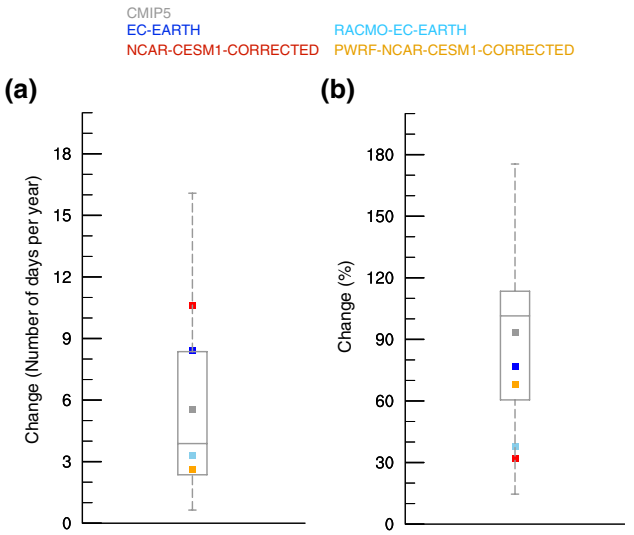

Fig. 14 **a** The same as Fig. 13 but for rain days. Rain days are defined as the days when daily precipitation ≥ 1 mm on melt days

5 Summary and concluding remarks

In this study, we assessed the near future (2020–2044) temperature and precipitation changes over the Antarctic Peninsula under the high-emission scenario (RCP8.5). We used historical and projected simulations from 19 global climate models (GCMs) participating in CMIP5. We compare and contrast GCMs projections with two groups of regional climate model simulations (RCMs): (1) high resolution (15-km) simulations performed with Polar-WRF model forced with bias-corrected boundary conditions obtained from NCAR-CESM1-CORRECTED (PWRF-NC-CORR) over the Antarctic Peninsula, (2) medium resolution (50-km) simulations of KNMI-RACMO21P forced with EC-EARTH (RACMO-EC) obtained from the CORDEX-Antarctica. Our key results can be summarized as follows:

- Near future temperature projections indicate that mean annual temperatures are projected to increase by about 0.5–1.5°C across the entire Peninsula. Temperature increase is more substantial in autumn and winter (~ 2 °C). The CMIP5 ensemble mean projects slightly larger temperature increases on the leeward side.
- Overall, RCM projections follow the same climate change signal depicted in the driving fields, except the NC-CORR and PWRF-NC-CORR paired simulations in winter on the leeward side, where PWRF-NC-CORR projects an increase in temperature unlike the driving field that shows a slight decrease signal.
- In terms of precipitation projections, there is a broad agreement among the simulations, indicating an increase in mean annual precipitation (~ 5 to 10%) over the Antarctic Peninsula. A more increase in summer precipitation confined to the cordillera in the RCM projections highlights the role of a finer detailed topography and orographic influences.
- Overall, similar to the temperature projections, RCM projections reproduce similar projected changes of precipitation to those in the driving fields. On the other hand, some differences such as opposite sign of the change between EC and RACMO-EC on the leeward side indicate the existence of potential added values introduced by RCMs with different physical configuration and topography.
- Each simulation projects increases in melt days in the Larsen Ice Shelf of about 4–20 days per year. Unlike the driving fields, both RCMs show smaller increases in melt days and rain days in the Larsen Ice Shelf.

Further research is required to assess the physical reasoning of RCM and GCM differences at local-scale by delving deeper into physical processes such as impact of sea-ice feedback, radiative fluxes, precipitation shadow and rain/snow ratio on the projections. Furthermore, given that RCM simulations are largely performed in stand-alone mode, reduced uncertainties of the sea-ice and SST fields in the GCMs can also contribute to have more robust assessments of the regional climate change projections.

Given the high computational costs of RCMs particularly over such complex terrain of Antarctica, development of CORDEX-like initiatives over the sub-Antarctic domains such as Antarctic Peninsula and West Antarctica can allow to implement different RCM strategies and model tuning, and thus, provide beneficial assessment strategies for the climate change projections at regional scales. Furthermore, as there are lack of high-resolution RCM projections over the Antarctic Peninsula, more RCM applications within these initiatives can improve the assessment of climate change uncertainties as well as our understanding of the added value introduced by the RCMs. Additional efforts such as evaluation and subsetting of GCMs with the aim of dynamical downscaling (e.g., Agosta et al. 2015) would also contribute to have a more robust range of simulations matrices (i.e., different RCMs forced with different GCMs) that can reduce the potential uncertainties.

Supplementary Information The online version supplementary material available at https://doi.org/10.1007/s00382-021-05667-2.

Acknowledgements This work was funded by ANID-FONDAP-15110009. Deniz Bozkurt acknowledges support from ANID-CONICYT-PAI-77190080, ANID-PIA-Anillo INACH ACT192057 and ANID-FONDECYT-11200101. Contribution number 1597 of Byrd Polar and Climate Research Center. David Bromwich was supported by NSF Grant 1823135. Jorge Carrasco acknowledges support from ANID-FONDECYT-1191932. Polar-WRF simulations were performed within a project entitled "Simulaciones climáticas regionales para el continente Antártico y territorio insular Chileno" funded by Chilean Ministry of Environment. This research was partially supported by the Basal Grant AFB 170001 and the supercomputing infrastructure of the NLHPC (ECM-02:Powered@NLHPC). We acknowledge the World Climate Research Programme,Working Group on Regional Climate, and the Working Group on Coupled Modelling, former coordinating body of CORDEX and responsible panel for CMIP5. We thank the NCAR for providing CESM data in WRF intermediate data format. We also thank the KNMI for producing and making available RACMO model output. The authors appreciate the support of Amazon Web Services (AWS) for the grants PS_R_FY2019_Q1_CR2 and PS_R_FY2019_Q2_CR2 allowing us to execute the Polar-WRF simulations on the AWS cloud infrastructure. We appreciate the support from Juan Carlos Maureira at Center for Mathematical Modeling, University of Chile for execution of model simulations. We are thankful to Francisca Muñoz, Nancy Valdebenito and Mirko Del Hoyo at CR2 for post-processing of Polar-WRF simulations.

References

Abram N, Mulvaney R, Vimeux F et al (2014) Evolution of the southern annular mode during the past millennium. Nat Clim Change 4:564–569. https://doi.org/10.1038/nclimate2235

Addor N, Rohrer M, Furrer R, Seibert J (2016) Propagation of biases in climate models from the synoptic to the regional scale: implications for bias adjustment. J Geophys Res Atmos 121:2075–2089. https://doi.org/10.1002/2015JD024040

Agosta C, Fettweis X, Datta R (2015) Evaluation of the CMIP5 models in the aim of regional modelling of the Antarctic surface mass balance. Cryosphere 9:2311–2321. https://doi.org/10.5194/tc-9-2311-2015

Bozkurt D, Rondanelli R, Marín J, Garreaud R (2018) Foehn event triggered by an atmospheric river underlies record-setting temperature along continental Antarctica. J Geophys Res Atmos 128(3):3871–3892. https://doi.org/10.1002/2017JD027796

Bozkurt D, Bromwich DH, Carrasco J, Hines KM, Maureira JC, Rondanelli R (2020) Recent near-surface temperature trends in the Antarctic Peninsula from observed, reanalysis and regional climate model data. Adv Atmos Sci 37:477–493. https://doi.org/10.1007/s00376-020-9183-x

Bracegirdle TJ, Connolley WM, Turner J (2008) Antarctic climate change over the twenty first century. J Geophys Res 113(D03):103. https://doi.org/10.1029/2007JD008933

Bromwich DH, Hines KM, Bai LS (2009) Development and testing of polar weather research and forecasting model: 2. Arctic Ocean J Geophys Res 114(D08):122. https://doi.org/10.1029/2008JD010300

Bromwich DH, Nicolas JP, Monaghan AJ, Lazzara MA, Keller LM, Weidner GA, Wilson AB (2013) Central West Antarctica among the most rapidly warming regions on Earth. Nature Geosci 6:139–145. https://doi.org/10.1038/ngeo1671

Bromwich DH, Nicolas JP, Monaghan AJ, Lazzara MA, Keller LM, Weidner GA, Wilson AB (2014) Corrigendum: Central West Antarctica among the most rapidly warming regions on Earth. Nat Geosci 7:76. https://doi.org/10.1038/ngeo2016

Bruyére CL, Monaghan AJ, Steinhoff DF, Yates D (2015) Bias-corrected CMIP5 CESM data in WRF/MPAS intermediate file format. NCAR Tech. Note NCAR/TN-515+STR, NCAR, Boulder

C3S (2017) ERA5: Fifth generation of ECMWF atmospheric reanalyses of the global climate. Copernicus Climate Change Service (C3S) Climate Data Store (CDS)

Cape MR, Vernet M, Skvarca P, Marinsek S, Scambos M, Domack E (2015) Foehn winds link climate-driven warming to ice shelf evolution in Antarctica. J Geophys Res Atmos 120(11):37–11057. https://doi.org/10.1002/2015JD023465

Carrasco JF (2013) Decadal changes in the near-surface air temperature in the western side of the Antarctic Peninsula. Atmos Clim Sci 3:275–281

Clem KR, Lintner BR, Broccoli AJ, Miller JR (2019) Role of the South Pacific convergence zone in West Antarctic decadal climate variability. Geophys Res Lett 46:6900–6909. https://doi.org/10.1029/2019GL082108

Convey P, Smith RIL (2006) Responses of terrestrial Antarctic ecosystems to climate change. Plant Ecol 182(1–2):1–10

Delhasse A, Kittel C, Amory C, Hofer S, van As D, Fausto SR, Fettweis X (2020) Brief communication: evaluation of the near-surface climate in ERA5 over the Greenland Ice Sheet. Cryosphere 14(3):957–965. https://doi.org/10.5194/tc-14-957-2020

Di Luca A, Elia R, Laprise R (2013) Potential for small scale added value of RCMs downscaled climate change signal. Clim Dyn 40(3–4):601–618. https://doi.org/10.1007/s00382-012-1415-z

Ding Q, Steig E, Battisti D, Kuttel M (2011) Winter warming in West Antarctica caused by central tropical Pacific warming. Nat Geosci 4:398–403. https://doi.org/10.1038/ngeo1129

Dong X, Wang Y, Hou S, Ding M, Yin B, Zhang Y (2020) Robustness of the recent global atmospheric reanalyses for Antarctic near-surface wind speed climatology. J Clim 33:4027–4043. https://doi.org/10.1175/JCLI-D-19-0648.1

Elvidge AD, Renfrew IA, King JC, Orr A, Lachlan-Cope TA, Weeks M, Gray SL (2015) Foehn jets over the Larsen C Ice Shelf, Antarctica. Q J R Meteorol Soc 141:698–713. https://doi.org/10.1002/qj.2382

Frieler K, Clark PU, He F, Buizert C, Reese R, Ligtenberg SR, Van den Broeke MR, Winkelmann R, Levermann A (2015) Consistent evidence of increasing Antarctic accumulation with warming. Nat Clim Change 5:348–352

Giorgi F, Jones C, Asrar GR (2009) Addressing climate information needs at the regional level: the CORDEX framework. WMO Bull 58:175–183

Gossart A, Helsen S, Lenaerts JT, Broucke SV, van Lipzig NP, Souverijns N (2019) An evaluation of surface climatology in state-of-the-art reanalyses over the Antarctic Ice Sheet. J Clim 32:6899–6915. https://doi.org/10.1175/JCLI-D-19-0030.1

Graham LP, Hagemann S, Simon J, Beniston M (2007) On interpreting hydrological change from regional climate models. Clim Change 81:97–122

Grassi B, Redaelli G, Visconti G (2006) A physical mechanism of the atmospheric response over Antarctica to decadal trends in tropical SST. Geophys Res Lett 33(L17):814. https://doi.org/10.1029/2006GL026509

Guttler I, Stepanov I, Branković C, Nikulin G, Jones C (2015) Impact of horizontal resolution on precipitation in complex orography simulated by the Regional Climate Model RCA3. Mon Weather Rev 143:3610–3627. https://doi.org/10.1175/MWR-D-14-00302.1

Hazeleger WC, Severijns C, Semmler T et al (2008) EC-Earth—a seamless earth-system prediction approach in action. Bull Am Meteorol Soc 91:1357–1364. https://doi.org/10.1175/2010BAMS2877.1

Hersbach H, Bell B, Berrisford P et al (2020) The ERA5 global reanalysis. Q J R Meteorol Soc. https://doi.org/10.1002/qj.3803

Hines KM, Bromwich DH (2008) Development and testing of Polar WRF. Part I: Greenland ice sheet meteorology. Mon Weather Rev 136:1971–1989

Hines KM, Bromwich DH, Bai LS, Barlage M, Slater AG (2011) Development and testing of Polar WRF. Part III: Arctic Land. J Clim 24:26–48. https://doi.org/10.1175/2010JCLI3460.1

Hoegh-Guldberg O, Jacob D, Taylor M, Bindi M, Brown S, Camilloni I, Diedhiou A, Djalante R, et al (2018) Impacts of 1.5°C global warming on natural and human systems. In:*Global warming of 1.5°C. An IPCC Special Report on the impacts of global warming of 1.5°C above pre-industrial levels and related global greenhouse gas emission pathways, in the context of strengthening the global response to the threat of climate change, sustainable development, and efforts to eradicate poverty*. Masson-Delmotte, V., P. Zhai, H.-O. Pörtner, D. Roberts, J. Skea, P.R. Shukla, A. Pirani, W. Moufouma-Okia, C. Pén, R. Pidcock, S. Connors, J.B.R. Matthews, Y. Chen, X. Zhou, M.I. Gomis, E. Lonnoy, T. Maycock, M. Tignor, and T. Waterfield (eds.)

Hosking JS, Orr A, Marshall GJ, Turner J, Phillips T (2013) The influence of the Amundsen–Bellingshausen Seas low on the climate of West Antarctica and its representation in coupled climate model simulations. J Clim 26:6633–6648. https://doi.org/10.1175/JCLI-D-12-00813.1

Hosking JS, Orr A, Bracegirdle TJ, Turner J (2016) Future circulation changes off West Antarctica: sensitivity of the Amundsen Sea Low to projected anthropogenic forcing. Geophys Res Lett 43:367–376. https://doi.org/10.1002/2015GL067143

Jones ME, Bromwich DH, Nicolas JP, Carrasco J, Plavcová Zou X, Wang SH (2019) Sixty years of widespread warming in the southern mid- and high-latitudes. J Clim 32:6875–6898. https://doi.org/10.1175/JCLI-D-18-0565.1

Jones PW (1999) First- and second-order conservative remapping schemes for grids in spherical coordinates. Mon Weather Rev 127:2204–2210

King JC, Turner J (2009) Antarctic meteorology and climatology. Cambridge University Press, Cambridge. https://doi.org/10.1017/CBO9780511524967

King JC, Gadian A, Kirchgaessner A et al (2015) Validation of the summertime surface energy budget of Larsen C Ice Shelf (Antarctica) as represented in three high-resolution atmospheric models. J Geophys Res Atmos 120:1335–1347. https://doi.org/10.1002/2014JD022604

Lenaerts JTM, Van den Broeke MR, Van de Berg WJ, Van Meijgaard E, Kuipers Munneke P (2012) A new, high-resolution surface mass balance map of Antarctica (1979–2010) based on regional atmospheric climate modeling. Geophys Res Lett 39(L04):501. https://doi.org/10.1029/2011GL050713

Liang XZ, Kunkel KE, Meehl GA, Jones RG, Wang JXL (2008) Regional climate models downscaling analysis of general circulation models present climate biases propagation into future change projections. Geophys Res Lett 35(L08):709. https://doi.org/10.1029/2007GL032849

Listowski C, Lachlan-Cope T (2017) The microphysics of clouds over the Antarctic Peninsula—Part 2: modelling aspects within Polar-WRF. J Geophys Res Atmos 17:10195–10221

Liu Y, Li F, Hao W, Barriot JP, Wang Y (2019) Evaluation of synoptic snowfall on the Antarctic Ice Sheet based on CloudSat, in-situ observations and atmospheric reanalysis datasets. Remote Sens 11(14):1686. https://doi.org/10.3390/rs11141686

Marshall GJ, Orr A, van Lipzig NPM, King JC (2006) The impact of a changing Southern Hemisphere annular mode on Antarctic Peninsula summer temperatures. J Clim 19(20):5388–5404. https://doi.org/10.1175/JCLI3844.1

Marshall GJ, Thompson DWJ, Van den Broeke MR (2017) The signature of Southern Hemisphere atmospheric circulation patterns in Antarctic precipitation. Geophys Res Lett 44:11580–11589. https://doi.org/10.1002/2017GL075998

Naughten KA, Meissner KJ, Galton-Fenzi BK, England MH, Timmermann R, Hellmer HH (2018) Future projections of Antarctic Ice Shelf melting based on CMIP5 scenarios. J Clim 31:5243–5261. https://doi.org/10.1175/JCLI-D-17-0854.1

Niu X, Wang S, Tang J, Lee DK, Gao X, Wu J, Hong S, Gutowski WJ, McGregor J (2015) Multimodel ensemble projection of precipitation in eastern China under A1B emission scenario. J Geophys Res Atmos 120:9965–9980. https://doi.org/10.1002/2015JD023853

Oliva M, Navarro F, Hrbacek F, Hernandez A, Nyvlt D, Pereira P, Ruiz-Fernandez J, Trigo R (2017) Recent regional climate cooling on the Antarctic Peninsula and associated impacts on the cryosphere. Sci Total Environ 580:210–223. https://doi.org/10.1016/j.scitotenv.2016.12.030

Palerme C, Genthon C, Claud C, Kay JE, Wood NB, L'Ecuyer T (2017) Evaluation of current and projected Antarctic precipitation in CMIP5 models. Clim Dyn 48:225–239. https://doi.org/10.1007/s00382-016-3071-1

Rignot E, Casassa G, Gogineni P, Krabill W, Rivera A, Thomas R (2004) Accelerated ice discharge from the Antarctic Peninsula following the collapse of Larsen B Ice Shelf. Geophys Res Lett 31(L18):401. https://doi.org/10.1029/2004GL020697

Rondanelli R, Hatchett B, Rutllant J, Bozkurt D, Garreuad R (2019) Strongest MJO on record triggers extreme Atacama rainfall and warmth in Antarctica. Geophys Res Lett 46(6):3482–3491. https://doi.org/10.1029/2018GL081475

Scambos TA, Bohlander JA, Human CA, Skvarca P (2004) Glacier acceleration and thinning after ice shelf collapse in the Larsen B embayment. Geophys Res Lett 31(L18):402. https://doi.org/10.1029/2004GL020670

Screen JA, Bracegirdle TJ, Simmonds I (2018) Polar climate change as manifest in atmospheric circulation. Curr Clim Change Rep 4:383–395. https://doi.org/10.1007/s40641-018-0111-4

Skamarock WC, Klemp JB, Dudhia J, Gill DO, Barker DM, Duda M, Huang XY, Wang W, Power JG (2008) A description of the advanced research WRF Version 3. NCAR Tech. Note NCAR/TN-475 + STR, NCAR, Boulder

Sørland SL, Schär C, Lüthi D, Kjellström E (2018) Bias patterns and climate change signals in GCM-RCM model chains. Environ Res Lett 13(074):017. https://doi.org/10.1088/1748-9326/aacc77

Taylor KE, Stouffer RJ, Meehl GA (2012) An overview of CMIP5 and the experiment design. Bull Am Meteorol Soc 93:485–498

Tetzner D, Thomas L, Allen C (2019) A validation of ERA5 reanalysis data in the southern Antarctic Peninsula-Ellsworth Land region, and its implications for ice core studies. Geosciences 9:289. https://doi.org/10.3390/geosciences9070289

Turner J, Bracegirdle TJ, Phillips T, Marshall GJ, Hosking JS (2013) An initial assessment of Antarctic sea ice extent in the CMIP5 models. J Clim 26:1473–1484. https://doi.org/10.1175/JCLI-D-12-00068.1

Turner J, Lu H, White I, King JC, Phillips JS, Hosking JS et al (2016) Absence of 21st century warming on Antarctic Peninsula consistent with natural variability. Nature 535:411–415. https://doi.org/10.1038/nature18645

Turner J, Guarino MV, Arnatt J, Jena B, Marshall GJ, Phillips T, Bajish CC, Clem K, Wang Z, Andersson T, Murphy EJ, Cavangh R (2020a) Recent decrease of summer sea ice in the Weddell Sea, Antarctica. Geophys Res Lett. https://doi.org/10.1029/2020GL087127

Turner J, Marshall GJ, Colwell S, Phillips T, Lu H (2020b) Antarctic temperature variability and change from station data. Int J Climatol 40:2986–3007. https://doi.org/10.1002/joc.6378

Van Den Broeke MR, Van Lipzig NPM (2004) Changes in Antarctic temperature, wind and precipitation in response to the Antarctic Oscillation. Ann Glaciol 39:119–126. https://doi.org/10.3189/172756404781814654

Van Lipzig NPM, Marshall GJ, Orr A, King JC (2008) The relationship between the Southern Hemisphere annular mode and Antarctic Peninsula summer temperatures: analysis of a high-resolution model climatology. J Clim 21(8):1649–1668. https://doi.org/10.1175/2007JCLI1695.1

Van Meijgaard E, van Ulft LH, van de Berg WJ, Bosvelt FC, van den Hurk BJJM, Lenderink G, Siebesma AP (2008) The KNMI regional atmospheric model RACMO version 2.1. Tech. Note Tech. Rep. 302, R. Neth. Meteorol. Inst., Netherlands

Van Wessem JM, Ligtenberg SRM, Reijmer CH, Van de Berg WJ, Van den Broeke MR, Barrand NE, Thomas ER, Turner J, Wuite J, Scambos TA, Van Meijgaard E (2016) The modelled surface mass balance of the Antarctic peninsula at 5.5 km horizontal resolution. Cryosphere 10:271–285. https://doi.org/10.5194/tc-10-271-2016

Wilby RL, Whitehead PG, Wade AJ, Butterfield D, Davis RJ, Watts G (2004) Integrated modelling of climate change impacts on water resources and quality in a lowland catchment: River Kennet, UK. J Hydrol 330:204–220

Wille JD, Favier V, Dufour A, Gorodetskaya IV, Turner J, Agosta C, Codron F (2019) West Antarctic surface melt triggered by atmospheric rivers. Nat Geosci 12:911–916

Wilson AB, Bromwich DH, Hines KM (2016) Simulating the mutual forcing of anomalous high-southern latitude atmospheric circulation by El Niño flavours and the Southern Annular Mode. J Clim 29(6):2291–2309. https://doi.org/10.1175/JCLI-D-15-0361.1

Zheng F, Li J, Clark RT, Nnamchi HC (2013) Simulation and projection of the Southern Hemisphere Annular Mode in CMIP5 models. J Clim 26:9860–9879. https://doi.org/10.1175/JCLI-D-13-00204.1